Ab Initio Modeling of the Spatial, Electronic, and Vibrational Structure of Schiff Base Models for Visual Photoreceptors

Sylvia I. E. Touw, Huub J. M. de Groot, and Francesco Buda*

Gorleaus Laboratories, Leiden Institute of Chemistry, Leiden University, P.O. Box 9502, 2300 RA Leiden, The Netherlands

Received: March 22, 2004; In Final Form: June 7, 2004

We have assessed the relation between the spatial ground-state structure and the electronic and vibrational spectroscopic properties of neutral and protonated 11-*cis*-retinal Schiff base models within the density functional theory framework. For the neutral Schiff base model, a comprehensive model picture emerges, which is consistent with the available spectroscopic experimental data. For the protonated models, the calculations reveal a polaronic conjugation defect in the ground state in the Schiff base region. It is found that the C_{14}—C_{15} bond has enhanced double bond character, while the C_{13}═C_{14} and C_{15}═N bonds have reduced double bond character. This phenomenon affects the vibrational structure in an extended region of the spectrum. The C—C, C═C, and C═N stretches in the fingerprint region and the ethylenic band are significantly delocalized. In the ab initio calculations, an enhanced coupling of the C_{14}—C_{15} and C_{15}═N stretching coordinates transpires, resulting in an asymmetric (C_{14}—C_{15}═N) stretching mode in the ethylenic region at 1639 cm^{-1}. In addition, a coupled $C_{14}H$—$C_{15}H$ A_u hydrogen-out-of-plane mode is found at 1019 cm^{-1}. The calculated ^{13}C NMR chemical shifts in the polyene chain are very sensitive to the perturbation of the bond length alternation pattern. The protonated models show a C_{13} response that is more deshielded than C_{15}, supporting the presence of a polaronic charge effect in the protonated Schiff base and an accumulation of charge at C_{13}, in line with all NMR spectroscopic data. Finally, we have resolved an essential difference between retinylidene iminium salts and rhodopsin. In contrast with rhodopsin, the delocalization of positive charge in these model compounds is intimately connected with the polarization effects from the counterion at the Schiff base. This supports recent inferences that the negative charge of the counterion in the rhodopsin protein is strongly delocalized around the polyene chain of the chromophore, and promotes accumulation of positive charge around the *cis* bond.

Introduction

Bovine rhodopsin is the photoreceptor protein that is responsible for dim light vision in vertebrates. The first step in the process of vision is an 11-*cis* to all-*trans* isomerization of the light-absorbing ligand in the active site of rhodopsin upon absorption of a photon.[1] This process is completed within 200 fs with a quantum yield of 0.67, and it is one of the fastest photochemical reactions.[2,3] It is characterized by a high efficiency in energy conversion, since 32−35 kcal/mol of the energy of the absorbed photon is stored in the primary photoproduct bathorhodopsin, a highly strained all-*trans* configuration of the chromophore.[1,4,5] The isomerization process is followed by a sequence of dark reactions in the protein that initiates the visual signal transduction cascade, and ultimately triggers a nerve pulse.[6]

Rhodopsin is located in the disk membrane of the outer segments of rod cells. It is a 40 kDa G-protein coupled receptor consisting of a polypeptide chain of 348 amino acids that is folded into seven transmembrane α-helical segments linked by hydrophilic loops.[7,8] The light-absorbing group in rhodopsin is a retinylidene group with a 6-s-*cis*-11-*cis*-12-s-*trans* conformation which is covalently bound to the protein by means of a protonated Schiff base (PSB) linkage to the ϵ-amino group of the Lys296 residue located in the seventh transmembrane segment (see Figure 1).[9−11] The protonation of the Schiff base introduces a positive charge in the chromophore. In the past, mutagenesis studies have indicated that the positive charge of the chromophore is neutralized by the carboxylate side chain of the Glu113 residue in helix III that serves as a counterion.[12−14] The electrostatic interactions between the chromophore and the counterion environment contribute to locking the protein in an inactive state in the dark, and tune the absorption properties of the chromophore in the visible region of the electromagnetic spectrum. Recently, X-ray crystallography revealed that the side chain of Glu113 is located in the vicinity of the Schiff base nitrogen, suggesting a direct contact between them.[9−11] From a ^{15}N MAS NMR study, experimental evidence has been found for a complex counterion in which the carboxylate side chain of the glutamate residue interacts with the proton on the Schiff base nitrogen via a hydrogen-bonded network.[15]

The 2.6 Å resolution of the most recently determined X-ray structure is insufficient for resolving the spatial structure of the retinylidene chromophore of rhodopsin in intramolecular detail.[11] At an early stage, solid-state NMR, FTIR, and resonance Raman spectroscopy have provided comprehensive information with respect to the structural and electronic properties of the 11-*cis*-retinal PSB chromophore that is complementary to the more recent X-ray and modeling.[2,16−22] The experimental data obtained with these spectroscopic techniques have been reproduced now in many cases and are considered unambiguous. In contrast,

* Corresponding author. E-mail: f.buda@chem.leidenuniv.nl.

10.1021/jp048734b CCC: $27.50
Published on Web 08/10/2004

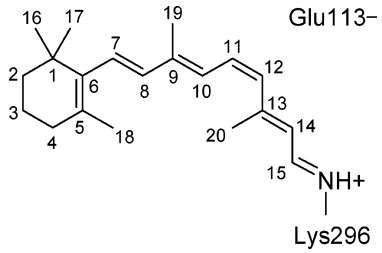

Figure 1. Molecular structure of the 11-*cis*-retinylidene chromophore in bovine rhodopsin. The numbering is in accordance to the International Union of Pure and Applied Chemistry rules for the Schiff base.

the theoretical interpretation of the data does not yet lead to a fully consistent molecular picture in terms of spatial, electronic, and vibrational structure. ^{13}C NMR experiments have revealed that C_{13} is more deshielded than C_{15} and that the downfield shift of C_{13} upon protonation exceeds the downfield shift of C_{15}.[16,23] This strongly supports the presence of a polaronic charge effect in the protonated Schiff base chromophore.[23] Car−Parrinello molecular dynamics (CPMD) studies on a minimal model of the rhodopsin PSB confirm that the positive charge in the chromophore introduces a self-localized conjugation defect in the polyene adjacent to the electronegative nitrogen atom.[24−30] An essential property of a conjugation defect is a decrease of the dimerization amplitude. In conjugated polyene chains, the dimerization amplitude $D_{i,j,k}$ is defined as the difference between adjacent carbon−carbon bond lengths, i.e.

$$D_{i,j,k} = d_{i,j} - d_{j,k} \quad (1)$$

where $d_{i,j}$ and $d_{j,k}$ denote the lengths of the C_i-C_j and C_j-C_k bonds, respectively. If $D_{i,j,k}$ and $D_{i+1,j+1,k+1}$ have the same sign, a conjugation defect is present in the polyene chain in the region between C_{i+1} and C_{k+1}.

In the region where the positive charge is localized in the 11-*cis*-retinal PSB, the lengths of a few double bonds increase, while the lengths of single bonds decrease. Consequently, the $C_{14}-C_{15}$ bond has significant double bond character, while the double bond character of the $C_{13}=C_{14}$ and $C_{15}=N$ bonds is substantially reduced. This is in line with CPMD and DFT modeling and has been reconciled with NMR shift data for rhodopsin.[23,26−29,31] A similar effect on the bond lengths is observed for retinylidene iminium salts with X-ray experiments.[32] The 2.6 Å resolution of the recently determined X-ray structure of rhodopsin is insufficient to be able to observe these small effects on C−C bond lengths.[11] Recently, bond-length perturbations in the rhodopsin chromophore have been studied directly by means of double-quantum solid-state NMR.[33] These experiments provide evidence for a different bonding pattern scheme and indicate that the reduction of the bond length alternation, and hence the positive charge, is situated preferentially in the region $C_{12}-C_{13}$. Thus, in contrast with the model compounds, the excess charge due to protonation of the Schiff base appears to hop over the C_{15} and settle nearly at C_{13}. In this respect, these NMR results are in agreement with resonance Raman data for rhodopsin: A mode at 1190 cm^{-1} has been assigned predominantly to the $C_{14}-C_{15}$ local mode stretch, at a low frequency in the fingerprint region compared to the other C−C stretches.[21] This suggests enhanced single bond character for $C_{14}-C_{15}$. Thus, an ambiguity has emerged. Earlier NMR and modeling studies suggest a partial double bond character for the $C_{14}-C_{15}$ bond, i.e., a penetration of a polaronic charge defect in the conjugated chain, while the resonance Raman data and the recent double-quantum solid-state NMR experiments converge toward single bond character for $C_{14}-C_{15}$. This is more in line with a polaronic charge defect hopping over the vicinity of the Schiff base.

The objective of this study is to resolve the contradictory picture emerging from the experimental data with the aid of ab initio calculations on simple model compounds. We present a comprehensive picture of the spatial, electronic, and vibrational structure of the model compounds that is consistent with results from ^{13}C solid-state NMR, resonance Raman, and X-ray experiments. By means of density functional theory (DFT) calculations on neutral and protonated 11-*cis*-retinal Schiff base models, we can evaluate the spatial, electronic, and vibrational properties within a single framework: in this way the possible origins of the contradictory picture emerging from the experimental data can be addressed more directly. In a first step, DFT is applied to calculate the ground-state spatial structure of the retinylidene model compounds.[34] In a second step, the NMR properties of the carbon atoms in the conjugated chains are evaluated through the calculation of the ^{13}C isotropic chemical shifts and the principal components of the corresponding chemical shift tensors. The normal mode vibrations of the Schiff base models are studied in a third step. Finally, the predictive range of density functional theory in the analysis of spatial, electronic, and vibrational structural properties is assessed, and a comparison of the theoretical results with the experimental data obtained with resonance Raman and NMR spectroscopy for model compounds and for rhodopsin is presented. An ab initio analysis of the normal mode vibrations for protonated Schiff base models has never been published before. In addition, for the first time the spatial, electronic, and vibrational properties of PSB model compounds are presented within a single theoretical framework.

Computational Methods

The ground-state equilibrium structure, the ^{13}C NMR chemical shift tensors, and the normal mode vibrations of the 11-*cis*-retinal PSB have been determined within the density functional theory framework.[34] The geometry optimization and the calculation of the normal mode vibrations have been performed using gradient corrections to the local density approximation (LDA) in the form proposed by Becke and Perdew (BP86).[35−37] This functional has been chosen for consistency with our previous work and to enable comparison of the resulting ground-state geometries with the geometries of our previous models.[26−29] Only the valence electrons have been treated explicitly. The interaction with the inner core electrons is described by using soft first-principles pseudopotentials in the form proposed by Vanderbilt.[38] The Kohn−Sham single particle wave functions are expanded on a plane wave basis set with an energy cutoff of 25 Rydberg. The expansion of the wave functions in terms of plane waves implies the use of periodic boundary conditions. The simulation box has been chosen $40 \times 25 \times 25$ au^3, which is sufficiently large to avoid interaction with the images.

The normal modes and vibrational frequencies of the optimized structure have been calculated by numerical differentiation of the forces with respect to the Cartesian nuclear coordinates, and a subsequent transformation to mass-weighted normal coordinates, using a harmonic oscillator approximation. Since this approach is only valid at a stationary point on the potential energy surface, the vibrational mode analysis was performed on the fully relaxed structure of the model compound for the 11-*cis*-retinylidene chromophore; i.e., no constraints have been imposed on the structure during the preceding geometry optimization.[39] The representation of the normal modes in internal coordinates has been obtained by applying the Wilson

FG method to the Cartesian force constant matrix resulting from the ab initio calculations.[40] The optimization of the electronic wave functions and the atomic positions has been performed using direct inversion in the interactive subspace (DIIS).[41]

The calculation of the nuclear magnetic shielding tensor has been performed within the density functional theory framework, using Becke's gradient corrected exchange functional and the Lee, Yang, and Parr correlation functional (B3LYP).[42,43] The calculations employed the gauge invariant atomic orbitals (GIAO) method with the 6-31G basis set.[40,45] The B3LYP functional is the most widely used functional for predicting NMR properties, and in combination with the small 6-31G basis set it provides a method that produces reliable ^{13}C chemical shifts at a reasonable cost. We have tested this functional and basis set on several isomers of retinal, and the results are found to agree well with the experimental data: For the isotropic ^{13}C chemical shifts of the conjugated carbon atoms, the rms error is 4.1 ppm, and the correlation coefficient is $\rho = 0.982$, which is considered sufficiently accurate for our purpose.[46] The isotropic ^{13}C chemical shifts δ_i, and the principle components of the chemical shift tensor δ_{11}, δ_{22}, and δ_{33}, are quoted in parts per million (ppm) relative to the ^{13}C chemical shift of tetramethylsilane (TMS), i.e., $\sigma_i = 194.42$ ppm. This value has been determined theoretically by applying the same level of theory on an isolated molecule of TMS.

The accuracy of the calculated vibrational frequencies and chemical shifts has been assessed by determining the correlation with the experimental values. For any physical quantity x, the correlation coefficient ρ between the values of calculated quantities x_c and experimental quantities x_m is defined as

$$\rho = \frac{\sum_{i=1}^{N} \Delta x_{m,i} \Delta x_{c,i}}{\sqrt{\sum_{i=1}^{N} \Delta x_{m,i}^2 \sum_{i=1}^{N} \Delta x_{c,i}^2}} \qquad (2)$$

In eq 2, $\Delta x_{m,i}$ is the deviation of the measured value from the mean experimental value. Similarly $\Delta x_{c,i}$ is the deviation of the calculated value from the mean calculated value.

The geometry optimizations and the calculation of the normal mode vibrations have been performed using the CPMD program package.[47] The nuclear magnetic shielding tensors have been calculated with Gaussian98.[48]

Results

Spatial Structure. To mimic the retinylidene chromophore in rhodopsin we used the chromophore model as extracted from the X-ray structure of Palczewski et al.[9] The retinylidene chromophore in this X-ray model has a 6-s-*cis*-12-s-*trans* conformation with a planar $C_{10}-C_{13}$ moiety. Further refinement of the rhodopsin X-ray structure has yielded a new chromophore model, which includes an out-of-plane distortion in the $C_{10}-C_{13}$ moiety with a $C_{10}-C_{11}-C_{12}-C_{13}$ dihedral angle of 7.9°.[10] This is more in line with insights gained by NMR spectroscopy and modeling studies, which converge toward a chromophore that is conformationally twisted in the isomerization region, due to intramolecular and intermolecular steric interactions.[17,49] The degree of twist in this part of the molecule is thought to determine the rate and efficiency of the 11-*cis* to all-*trans* isomerization. We have started from the X-ray structure containing the more relaxed chromophore, based on energy considerations. Calculation of the total energy of both chromophore models within the DFT framework has revealed that the original X-ray model has an energy that is 0.065 au lower than that of the refined structure.

Following our earlier work, we have imposed some modifications on the X-ray structure in line with results of CP/MAS NMR experiments, i.e., $C_{10}-C_{20} \sim 3.0$ Å and $C_{11}-C_{20} \sim 2.9$ Å.[9,17] In addition, we have introduced an initial torsional angle of 15° in the $C_{10}-C_{13}$ segment. The chromophore model has been terminated with a CH_3 group to match the linkage of the protonated Schiff base to the Lys296 residue of the protein (see Figure 1). The Glu113 residue of the protein, which serves as a counterion, has been modeled by including an acetate ion (CH_3COO^-) in our model, with one oxygen atom of the carboxylate group placed at ~3 Å from C_{12} and the other at ~4.3 Å from N, in accordance with experimental NMR data.[15,50] In the X-ray model of Palczewski et al., the N−Glu113 distance is 0.322 nm.[9] We have tested this model and found that the proton is not stable on the nitrogen atom in the original configuration. During a geometry optimization, it moves toward the oxygen atom of the Glu113 residue. The $C_{12}-$Glu113 distance in the X-ray structure is 0.515 nm.[9] The stabilization of the positive charge on the chromophore is determined by its counterion environment. Very recently, it has been suggested that the Thr94 residue forms a hydrogen bond with the Glu113 residue, thus stabilizing the positive charge on the chromophore.[51] Water molecules in the vicinity of the counterion also might play a role in this respect. A recent molecular dynamics study suggested that the Glu181 residue located close to the 11-*cis* bond bears a negative charge.[52] To account for the electrostatic and steric interactions with the surrounding protein and prevent planarization of the structure, we have performed an initial geometry optimization on our input model, during which several constraints have been imposed. We have fixed the positions of the carbon atoms of the methyl group attached to the β-ionone ring to the experimental geometry, because the methyl groups are clearly visible in the X-ray diffraction map and their positions are therefore assumed to be well-determined. Reconstitution studies and solid-state NMR experiments have provided evidence for specific protein−ligand interactions, which are thought to be essential for the positioning of the β-ionone ring and in particular the methyl groups.[31,53] In addition, we fixed the positions of the carbon and oxygen atoms of the counterion and the carbon atom of the methyl group terminating the protonated Schiff base. The resulting structure served as a starting point for a subsequent geometry optimization in which all the constraints have been released. Similar optimizations have been performed on a neutral 11-*cis*-retinal SB model and a positively charged 11-*cis*-retinal PSB model without a counterion.

Figure 2 shows the resulting ground-state equilibrium structure of the 11-*cis*-retinal PSB + CH_3COO^- model compound from two different points of view. It has a 6-s-*cis*-12-s-*trans* conformation and is nonplanar in the isomerization region. The out-of-plane deformation is distributed along several bonds in the C_8-C_{14} region, the total torsion being approximately 22°. This is smaller than the 44° angle found in the earlier modeling results which were based on NMR distance measurements, and where a large error margin in the modeling procedure was present.[17−19] In addition, the resulting torsion of the ab initio calculations strongly depend on the initial geometry, and the initial constraints in the geometry optimization. Only an explicit inclusion of the protein environment in the model can give a more accurate estimate of the torsion.[51] The chirality of the

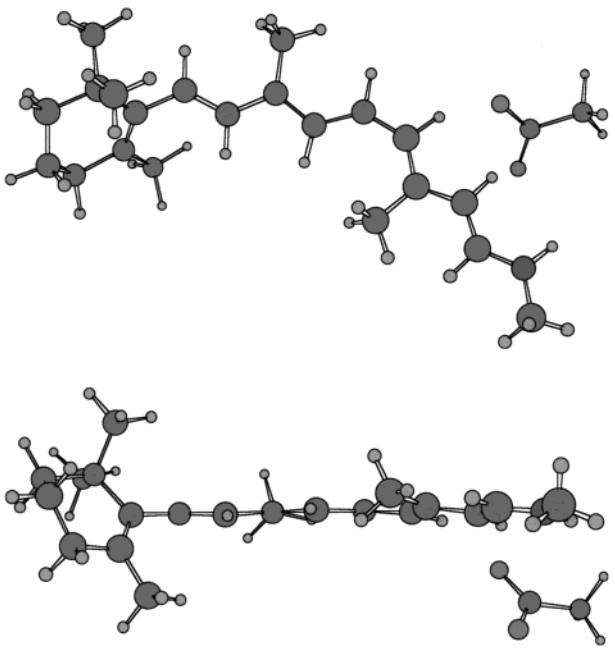

Figure 2. Ground-state equilibrium structure of the 11-*cis*-retinal PSB + CH_3COO^- model compound from two different points of view.

TABLE 1: Calculated Carbon−Carbon and Carbon−Nitrogen Bond Lengths in the Conjugated Chain of the Neutral 11-*cis*-Retinal Schiff Base (SB) and the 11-*cis*-Retinal Protonated Schiff Base (PSB) Model Compounds for the Retinylidene Chromophore of Rhodopsin with and without a CH_3COO^- Counterion

bond	SB	PSB	PSB + CH_3COO^-
C5═C6	1.354	1.372	1.360
C6−C7	1.492	1.459	1.477
C7═C8	1.357	1.379	1.367
C8−C9	1.463	1.440	1.450
C9═C10	1.374	1.407	1.395
C10−C11	1.436	1.402	1.413
C11═C12	1.365	1.402	1.397
C12−C13	1.464	1.411	1.414
C13═C14	1.365	1.416	1.415
C14−C15	1.447	1.379	1.378
C15═N	1.287	1.349	1.353

structure is in agreement with experimental results from circular dichroism spectroscopy.[54]

Table 1 reports the calculated carbon−carbon bond lengths in the polyene chain of the optimized structures of the 11-*cis*-retinal PSB model compounds. For comparison, the corresponding bond lengths in the neutral 11-*cis*-retinal SB are also shown.

Electronic Structure. We have calculated the ^{13}C NMR chemical shifts using density functional theory. The ^{13}C magnetic shielding tensors of the rhodopsin chromophore contain valuable information with respect to the electronic structure, complementary to the isotropic shift. To obtain this additional information, we have calculated the ^{13}C magnetic shielding tensors within the density functional theory framework. The calculated principal Cartesian components of the ^{13}C chemical shift tensor and the corresponding isotropic shifts of the carbon atoms in the conjugated chain of the model compounds are reported in Table 2.

Vibrational Structure. A DFT vibrational analysis of the 11-*cis*-retinal SB and PSB model compounds was performed to complement the chemical shift results. The most intense bands are observed in the 750−1700 cm^{-1} frequency region in the resonance Raman spectrum of rhodopsin. The low-frequency region of the spectrum contains the skeletal vibrations of the chromophore that could be correlated to the isomerization mechanism. Specifically, low-frequency skeletal modes with periods on the same time scale of the photoisomerization reaction, i.e., 200 fs, are important in this respect.[2] Since our 11-*cis*-retinal PSB model compounds do not describe the rhodopsin chromophore in its surrounding protein environment accurately, we do not expect reliable quantitative frequency predictions for the RR spectrum of rhodopsin, and theoretical identification of the low-frequency modes is therefore limited. However, since the vibrational character of these modes is also difficult to assess experimentally, we report a selection of the normal modes in the low-frequency region resulting from our theoretical analysis. We have selected the normal modes involving the $C_{10}-C_{11}-C_{12}-C_{13}$ torsional coordinate, which are directly relevant to the isomerization. For the neutral 11-*cis*-retinal SB, these low-frequency vibrational modes are presented in Table 3a. Tables 4a and 5a present similar normal modes for the 11-*cis*-retinal PSB and 11-*cis*-retinal PSB + CH_3COO^- model compounds, respectively. The most relevant calculated vibrational frequencies, and the descriptions of the corresponding normal modes in terms of contributing internal coordinates, of the neutral 11-*cis*-retinal SB model in the hydrogen-out-of-plane (HOOP) region, the fingerprint region, and the ethylenic band are reported in Table 3b−d, respectively. The corresponding results of the vibrational mode analysis of the positively charged 11-*cis*-retinal PSB model are given in Table 4b−d. Finally, Table 5b−d reports the resulting data of the vibrational mode analysis of the 11-*cis*-retinal PSB + CH_3COO^- model compound.

According to our calculations, all normal modes consist of contributions from several local coordinates, and in particular for the response in the fingerprint region the delocalization of the C−C stretches is very pronounced. The experimental peaks have been assigned in terms of a superposition of a few local coordinates based on extensive research involving measurements on several specific isotopically labeled rhodopsin analogues.[20−22] For comparison, we have assigned the observed frequencies to specific calculated normal modes of the 11-*cis*-retinal PSB + CH_3COO^- model compound. Since our calculations do not include Raman intensities, the assignment must be done with some caution. For the HOOP vibrations or hydrogen wags observed in the 750−1000 cm^{-1} frequency range, the ab initio calculations reveal that these modes have a relatively localized character, and hence, a description in terms of a few local

TABLE 2: Calculated Principal Cartesian Components of the ^{13}C Chemical Shift Tensor in the Conjugated Chain of the Neutral 11-*cis*-Retinal Schiff Base (SB) and the 11-*cis*-Retinal Protonated Schiff Base (PSB) Model Compounds for the Retinylidene Chromophore of Rhodopsin with and without a CH_3COO^- Counterion[a]

carbon atom	SB				PSB				PSB + CH_3COO^-			
	δ_{11}	δ_{22}	δ_{33}	δ_{iso}	δ_{11}	δ_{22}	δ_{33}	δ_{iso}	δ_{11}	δ_{22}	δ_{33}	δ_{iso}
C_5	219	143	30	130.5	239	196	30	154.8	217	160	31	135.9
C_6	225	138	57	139.7	225	155	51	143.6	224	139	52	138.6
C_7	215	138	29	127.0	245	179	27	150.3	226	151	28	135.2
C_8	227	126	62	138.1	216	136	54	135.0	220	131	56	135.8
C_9	217	156	28	133.8	240	215	30	161.9	227	184	32	147.6
C_{10}	212	130	49	130.0	198	141	42	127.0	205	142	42	129.4
C_{11}	219	127	28	124.6	239	162	25	142.1	230	158	25	137.6
C_{12}	224	133	45	134.1	202	118	43	120.9	214	151	29	131.2
C_{13}	237	153	33	141.1	234	221	29	161.1	235	220	31	161.9
C_{14}	213	120	49	127.5	167	118	45	110.1	175	154	33	120.7
C_{15}	247	146	64	152.3	231	161	54	148.8	229	154	58	146.9

[a] All values are reported in ppm relative to TMS.

TABLE 3: Normal Mode Vibrations of the 11-*cis*-Retinal SB

freq [cm^{-1}]		
calcd	exptl	normal mode description
		(a) In the Low-Frequency Region
131		$-0.103(C_{10}-C_{11}-C_{12}-C_{13}) - 0.120(C_{11}-C_{12}-C_{13}-C_{14}) - 0.111(C_{12}-C_{13}-C_{14}-C_{15}) - 0.170(C_{11}-C_{12}-C_{13}-C_{20}) - 0.100(C_{13}-C_{14}-C_{15}-N) + 0.128(C_5-C_6-C_7-H) + 0.117(C_6-C_7-C_8\text{-}H) - 0.101(C_{13}-C_{14}-C_{15}-H) + C_{13}$-methyl + β-ionone vibrations + lysine vibrations
136		$-0.130(C_{10}-C_{11}-C_{12}-C_{13}) - 0.112(C_{11}-C_{12}-C_{13}-C_{14}) - 0.103(C_{12}-C_{13}-C_{14}-C_{15}) - 0.140(C_{11}-C_{12}-C_{13}-C_{20}) + C_9$-methyl + C_{13}-methyl + β-ionone vibrations + lysine vibrations
226		$-0.112(C_7-C_8-C_9-C_{10}) - 0.156(C_{10}-C_{11}-C_{12}-C_{13}) - 0.107(C_{11}-C_{12}-C_{13}-C_{14}) + 0.170(C_{13}-C_{14}-C_{15}-N) + 0.131(C_9-C_{10}-C_{11}-H) + 0.190(C_{13}-C_{14}-C_{15}-H) + C_9$-methyl
341		$-0.147(C_5-C_6-C_7-C_8) + 0.208(C_7-C_8-C_9-C_{10}) - 0.191(C_9-C_{10}-C_{11}-C_{12}) - 0.203(C_{10}-C_{11}-C_{12}-C_{13}) - 0.198(C_{11}-C_{12}-C_{13}-C_{14}) - 0.105(C_{11}-C_{12}-C_{13}-C_{20}) - 0.101(C_5-C_6-C_7\text{-}H) - 0.136(C_6-C_7-C_8-H) + 0.172(C_8-C_9-C_{10}-H) + 0.162(C_{13}-C_{14}-C_{15}-H) + C_9$-methyl + β-ionone vibrations
387		$-0.134(C_7-C_8-C_9-C_{10}) - 0.101(C_9-C_{10}-C_{11}-C_{12}) + 0.104(C_{10}-C_{11}-C_{12}-C_{13}) + 0.134(C_{11}-C_{12}-C_{13}-C_{14}) - 0.125(C_{13}-C_{14}-C_{15}\text{-}N) - 0.130(C_8-C_9-C_{10}-H) + C_{13}$-methyl + β-ionone vibrations + lysine vibrations
499		$0.103(C_8-C_9-C_{10}) - 0.157(C_5-C_6-C_7-C_8) + 0.106(C_7-C_8-C_9-C_{10}) + 0.137(C_8-C_9-C_{10}-C_{11}) + 0.111(C_9-C_{10}-C_{11}-C_{12}) + 0.114(C_{10}-C_{11}-C_{12}-C_{13}) + 0.233(C_{11}-C_{12}-C_{13}-C_{14}) + 0.109(C_{12}-C_{13}-C_{14}-C_{15}) - 0.282(C_5-C_6-C_7\text{-}H) - 0.187(C_6-C_7-C_8-H) + 0.156(C_8-C_9-C_{10}-H) + 0.293(C_9-C_{10}-C_{11}-H) + 0.201(C_{12}-C_{13}-C_{14}-H) + 0.261(C_{13}-C_{14}-C_{15}-H) + C_9$-methyl + C_{13}-methyl + β-ionone vibrations + lysine vibrations
554		$-0.116(C_{13}-C_{14}-C_{15}) - 0.153(C_9-C_{10}-C_{11}-C_{12}) - 0.100(C_{10}-C_{11}-C_{12}-C_{13}) - 0.112(C_{11}-C_{12}-C_{13}-C_{14}) + 0.141(C_{13}-C_{14}-C_{15}-N) + 0.104(C_6-C_7-C_8-H) + 0.127(C_8-C_9-C_{10}-H) + 0.126(C_{13}-C_{14}-C_{15}-H) + C_9$-methyl + β-ionone vibrations + lysine vibrations
		(b) In the HOOP Region
796		$0.179(C_9-C_{19}) - 0.105(C_9-C_{10}-C_{11}-C_{12}) + 0.103(C_5-C_6-C_7\text{-}H) - 0.326(C_9-C_{10}-C_{11}\text{-}H) - 0.322(C_{10}-C_{11}-C_{12}-H) + C_{13}$-methyl: assignment ($C_{11}H{=}C_{12}H$ B_2 HOOP) − C_7H wag
829		$0.098(C_{13}-C_{20}) - 0.077(C_9-C_{10}-C_{11}) - 0.112(C_8-C_9-C_{10}-C_{11}) + 0.113(C_{10}-C_{11}-C_{12}-C_{13}) - 0.127(C_8-C_9-C_{10}-H) + 0.367(C_9-C_{10}-C_{11}-H) + 0.834(C_{10}-C_{11}-C_{12}-H) + C_{13}$-methyl: assignment $C_{12}H$ wag + $C_{11}H$ wag
860		$0.092(C_8-C_9) + 0.157(C_9-C_{19}) - 0.161(C_{10}-C_{11}-C_{12}) + 0.123(C_{11}-C_{12}-C_{13}) - 0.195(C_6-C_7-C_8-C_9) - 0.108(C_{11}-C_{12}-C_{13}-C_{14}) + 0.113(C_5-C_6-C_7\text{-}H) - 0.139(C_6-C_7-C_8-H) + C_9$-methyl + C_{13}-methyl + β-ionone vibrations
879		$-0.124(C_9-C_{19}) + 0.173(C_6-C_7-C_8) + 0.113(C_7-C_8-C_9) + 0.133(C_4-C_5-C_6-C_7) - 0.172(C_5-C_6-C_7-C_8) + 0.261(C_7-C_8-C_9-C_{10}) + 0.105(C_8-C_9-C_{10}-C_{11}) + 0.155(C_5-C_6-C_7-H) + 0.282(C_6-C_7-C_8-H) - 0.146(C_8-C_9-C_{10}-H) + C_9$-methyl + β-ionone vibrations: assignment ($C_7H{=}C_8H$ B_g HOOP) − $C_{10}H$ wag
882		$0.109(C_5-C_6-C_7-C_8) - 0.172(C_7-C_8-C_9-C_{10}) - 0.335(C_5-C_6-C_7\text{-}H) - 0.204(C_6-C_7-C_8-H) + 0.194(C_8-C_9-C_{10}-H) + \beta$-ionone vibrations: assignment ($C_7H{=}C_8H$ B_g HOOP) − $C_{10}H$ wag
899		$-0.161(C_5-C_6-C_7-H) + 0.138(C_8-C_9-C_{10}-H) + \beta$-ionone vibrations
911		$-0.101(C_{13}-C_{14}-H) - 0.305(C_8-C_9-C_{10}-H) - 0.288(C_{12}-C_{13}-C_{14}-H) + 0.120(C_{14}-C_{15}-N) +$ lysine vibrations
914		$-0.153(C_5-C_6-C_7-H) - 0.623(C_8-C_9-C_{10}-H) +$ lysine vibrations: assignment $C_{10}H$ wag
924		$0.129(C_5-C_6-C_7) + 0.413(C_5-C_6-C_7-H) + 0.263(C_8-C_9-C_{10}-H) + \beta$-ionone vibrations: assignment C_7H wag + $C_{10}H$ wag
927		$0.129(C_{11}-C_{12}-C_{13}-C_{14}) - 0.159(C_{13}-C_{14}-C_{15}-N) - 0.149(C_9-C_{10}-C_{11}-H) - 0.868(C_{12}-C_{13}-C_{14}-H) + C_{13}$-methyl: assignment $C_{14}H$ wag
965		$-0.143(C_9-C_{10}-C_{11}-C_{12}) - 0.155(C_{11}-C_{12}-C_{13}-C_{14}) - 0.099(C_5-C_6-C_7-H) + 0.110(C_6-C_7-C_8-H) - 0.148(C_8-C_9-C_{10}-H) + 0.658(C_9-C_{10}-C_{11}-H) - 0.535(C_{10}-C_{11}-C_{12}-H) - 0.179(C_{12}-C_{13}-C_{14}-H) + C_{13}$-methyl: assignment ($C_{11}H{=}C_{12}H$ A_2 HOOP) − $C_{14}H$ wag
983		$0.440(C_5-C_6-C_7-H) - 0.800(C_6-C_7-C_8-H) - 0.183(C_8-C_9-C_{10}-H) + C_9$-methyl: assignment ($C_7H{=}C_8H$ A_U HOOP)
985		$-0.098(C_{12}-C_{13}-C_{14}-C_{15}) - 0.197(C_{13}-C_{14}-C_{15}-N) - 0.101(C_{12}-C_{13}-C_{14}-H) + 0.674(C_{13}-C_{14}-C_{15}-H) +$ lysine vibrations: assignment $C_{15}H$ wag
		(c) In the Fingerprint Region[a]
1099	1100	$-0.162(C_{10}-C_{11}) + 0.130(C_9-C_{10}-C_{11}) + 0.152(C_{10}-C_{11}-C_{12}) - 0.115(C_{11}-C_{12}-H) + 0.181(C_8-C_9-C_{10}-C_{11}) + 0.177(C_8-C_9-C_{10}-H) - 0.115(C_{10}-C_{11}-C_{12}-H) + C_9$-methyl + C_{13}-methyl + β-ionone vibrations
1120		$0.117(C_6-C_7) + 0.101(C_6-C_7-H) + C_{13}$-methyl + β-ionone + lysine vibrations
1122		$-0.178(C_6-C_7) - 0.170(C_6-C_7-H) + 0.145(C_4-C_5-C_6-C_7) - 0.098(C_6-C_7-C_8-H) + C_{13}$-methyl + β-ionone + lysine vibrations
1151		$-0.164(C_4-C_5-C_6-C_7) - 0.094(C_5-C_6-C_7-H) + \beta$-ionone vibrations
1155	1157	$0.114(C_{10}-C_{11}) - 0.108(C_{12}-C_{13}) + 0.233(C_{14}-C_{15}) - 0.112(C_{13}-C_{14}-C_{15}) - 0.155(C_{14}-C_{15}-N) + 0.126(C_{10}-C_{11}-H) + 0.102(C_{11}-C_{12}-H) + 0.295(C_{14}-C_{15}\text{-}H) - 0.112(C_8-C_9-C_{10}-C_{11}) + 0.225(C_{12}-C_{13}-C_{14}-C_{15}) - 0.103(C_8-C_9-C_{10}-H) + 0.249(C_{12}-C_{13}-C_{14}-H) + C_{13}$-methyl + lysine vibrations
1184	1209	$-0.124(C_{12}-C_{13}) - 0.101(C_{14}-C_{15}) + 0.122(C_{12}-C_{13}-C_{14}) + 0.179(C_{13}-C_{14}-C_{15}) + 0.170(C_{14}-C_{15}-N) + 0.195(C_{10}-C_{11}-H) + 0.339(C_{13}-C_{14}-H) - 0.114(C_{14}-C_{15}-H) - 0.102(C_8-C_9-C_{10}-C_{11}) - 0.102(C_8-C_9-C_{10}-H) + C_{13}$-methyl + β-ionone + lysine vibrations
1188		$-0.174(C_5-C_6-C_7) + 0.105(C_{10}-C_{11}-H) + 0.202(C_{13}-C_{14}-H) + 0.143(C_4-C_5-C_6-C_7) + C_{13}$-methyl + β-ionone vibrations
1210		$0.114(C_6-C_7-H) + \beta$-ionone vibrations
1222		$-0.116(C_{13}-C_{14}-H) + \beta$-ionone vibrations
1226	1209	$0.179(C_8-C_9) - 0.135(C_9-C_{19}) - 0.117(C_7-C_8-C_9) - 0.167(C_8-C_9-C_{10}) - 0.140(C_9-C_{10}-C_{11}) - 0.237(C_9-C_{10}-H) - 0.197(C_{10}-C_{11}-H) + 0.245(C_{11}-C_{12}-H) + 0.306(C_{13}-C_{14}-H) + 0.158(C_8-C_9-C_{10}-C_{11}) + 0.151(C_8-C_9-C_{10}-H) + C_9$-methyl + β-ionone vibrations
1252		$0.354(C_6-C_7-H) + 0.184(C_{10}-C_{11}-H) - 0.124(C_{11}-C_{12}-H) - 0.194(C_{13}-C_{14}-H) - 0.103(C_{14}-C_{15}-H) + \beta$-ionone vibrations
1259	1267	$-0.117(C_{10}-C_{11}) + 0.135(C_8-C_9-C_{10}) + 0.142(C_9-C_{10}-C_{11}) - 0.111(C_{11}-C_{12}-C_{13}) - 0.143(C_{12}-C_{13}-C_{14}) + 0.116(C_6-C_7-H) - 0.392(C_{10}-C_{11}-H) + 0.208(C_{11}-C_{12}-H) + 0.392(C_{13}-C_{14}-H) + 0.245(C_{14}-C_{15}-H) + C_9$-methyl + β-ionone vibrations
1269		$0.141(C_{14}-C_{15}-H) +$ lysine vibrations
1281		$0.138(C_6-C_7) - 0.098(C_8-C_9) - 0.110(C_5-C_6-C_7) - 0.696(C_6-C_7\text{-}H) - 0.150(C_7-C_8-H) + 0.101(C_{10}-C_{11}-H) + 0.135(C_6-C_7-C_8-C_9) + \beta$-ionone vibrations
1295		$0.118(C_6-C_7-H) + \beta$-ionone vibrations

TABLE 3 (Continued)

freq [cm^{-1}]		
calcd	exptl	normal mode description
		(d) In the Ethylenic Band[b]
1530		$-0.225(C_9{=}C_{10}) + 0.249(C_{11}{=}C_{12}) - 0.117(C_{13}{=}C_{14}) - 0.136(C_8{-}C_9{-}C_{19}) + 0.170(C_6{-}C_7{-}H) + 0.186(C_9{-}C_{10}{-}H) + 0.132(C_{10}{-}C_{11}\text{-}H) - 0.288(C_{11}{-}C_{12}{-}H) + 0.154(C_{13}{-}C_{14}\text{-}H) - 0.132(C_{10}{-}C_{11}{-}C_{12}{-}C_{13}) + 0.101(C_{12}{-}C_{13}{-}C_{14}{-}C_{15}) + C_{13}$-methyl
1582		$-0.184(C_7{=}C_8) + 0.143(C_{12}{-}C_{13}) - 0.308(C_{13}{=}C_{14}) + 0.109(C_{14}{-}C_{15}) - 0.222(C_6{-}C_7{-}H) + 0.233(C_7{-}C_8{-}H) + 0.162(C_{11}{-}C_{12}{-}H) + 0.299(C_{13}{-}C_{14}{-}H) + C_{13}$-methyl
1587	1580	$0.206(C_7{=}C_8) - 0.166(C_8{-}C_9) + 0.243(C_9{=}C_{10}) - 0.160(C_{10}{-}C_{11}) + 0.104(C_{11}{=}C_{12}) - 0.110(C_{13}{=}C_{14}) + 0.213(C_6{-}C_7{-}H) - 0.324(C_7{-}C_8{-}H) - 0.313(C_9{-}C_{10}{-}H) + 0.294(C_{10}{-}C_{11}{-}H) + 0.101(C_{13}{-}C_{14}{-}H) + C_9$-methyl
1600		$-0.210(C_7{=}C_8) + 0.114(C_9{=}C_{10}) - 0.183(C_{10}{-}C_{11}) + 0.248(C_{11}{=}C_{12}) - 0.128(C_{12}{-}C_{13}) + 0.116(C_{13}{=}C_{14}) + 0.122(C_{12}{-}C_{13}{-}C_{20}) - 0.243(C_6{-}C_7{-}H) + 0.256(C_7{-}C_8{-}H) - 0.254(C_9{-}C_{10}{-}H) + 0.369(C_{10}{-}C_{11}{-}H) - 0.181(C_{11}{-}C_{12}{-}H) - 0.102(C_{13}{-}C_{14}{-}H) - 0.101(C_{10}{-}C_{11}{-}C_{12}{-}C_{13}) + C_{13}$-methyl
1625		$0.383(C_5{=}C_6) - 0.163(C_6{-}C_7{-}H) - 0.130(C_6{-}C_7{-}C_8{-}C_9) + \beta$-ionone vibrations
1635	1632	$-0.190(C_{14}{-}C_{15}) + 0.358(C_{15}{=}N) - 0.117(C_{13}{-}C_{14}{-}C_{15}) - 0.163(C_{13}{-}C_{14}{-}H) + 0.504(C_{14}{-}C_{15}{-}H)$

[a] Experimental values from ref 21. [b] Experimental values from ref 54.

coordinates appears adequate. The normal mode calculated at 1053 cm^{-1} is the $C_7H{=}C_8H$ A_u HOOP mode. This HOOP mode has been detected experimentally at 976 cm^{-1}. Since the calculations do not reveal any other $C_7H{=}C_8H$ HOOP mode with the same symmetry, the assignment is rather trivial. A similar argument holds for the assignment of the $C_{11}H{=}C_{12}H$ A_u HOOP, which has been calculated at 1056 cm^{-1}. This mode can be unambiguously assigned to the peak detected at 970 cm^{-1} in the Raman spectrum of rhodopsin. Finally, a strong peak has been detected at 843 cm^{-1}, which has been assigned to the $C_{10}H$ wag in combination with the $C_7H{=}C_8H$ B_g HOOP mode. The DFT calculations reveal several normal modes with a contribution of the $C_{10}H$ wag. Its relative amplitude is largest at 993 cm^{-1}, and at this frequency it appears in combination with the $C_7H{=}C_8H$ B_g HOOP mode. Therefore, we have assigned this calculated mode to the experimental peak observed at 843 cm^{-1}.

The peaks observed in the ethylenic band at 1548 and 1653 cm^{-1}, corresponding to the C=C in phase stretch and the C=N stretch, respectively, can be assigned unambiguously to the modes calculated at 1561 and 1639 cm^{-1}. Assignment of the peaks observed in the fingerprint region of the Raman spectrum to specific calculated normal modes, however, is less straightforward. As a criterion, we have assigned the peak identified as a specific C−C stretch in the Raman spectrum to the calculated vibrational mode containing the largest component of that C−C stretch. The assignments are given in Table 5a−c. For the neutral 11-*cis*-retinal SB, we assigned the observed frequencies in the fingerprint region to specific calculated normal modes using the same criterion.[21] The results are given in Table 3b. There are no experimental data available for the neutral 11-*cis*-retinal SB in the HOOP region and the ethylenic band. The experimental data of the ethylenic band, given in Table 3c, refer to the all-*trans* isomer of the neutral SB.[55]

Discussion

Spatial Structure. Table 1 reveals that the 11-*cis*-retinal PSB + CH_3COO^- model compound presents a significant disturbance of the bond length alternation pattern in the terminal region adjacent to the electronegative nitrogen: the lengths of the double bonds increase and the lengths of the single bonds decrease relative to an unperturbed conjugated chain. This is also evident from Figure 3, which shows the dimerization amplitude as a function of carbon atom label *j* in the conjugated chain of the neutral 11-*cis*-retinal SB and the positively charged model compounds. In the neutral 11-*cis*-retinal SB, the sign of the dimerization amplitude clearly alternates between adjacent C−C bonds in the conjugated chain. The 11-*cis*-retinal PSB model compounds exhibit a reduced dimerization amplitude in the region between C_{10} and C_{15}. This reduction in the dimerization amplitude can be attributed to the delocalization of the positive charge introduced in the chromophores by the protonation of the Schiff base. In our PSB + CH_3COO^- model compound, the decreased dimerization amplitude represents a conjugation defect in the polyene chain, with a double/single bond alternation switching at the C_{13}. As a result, the $C_{14}{-}C_{15}$ bond has significant double bond character, while the double bond character of the $C_{13}{=}C_{14}$ and $C_{15}{=}N$ bonds is strongly reduced. This matches the high-resolution crystal structures of *N-tert*-butyl-retinylideniminium perchlorate, which is chemically analogous to the rhodopsin chromophore, except for the bond conformation and for the different molecular environment. A strong reduction in bond length alternation is observed at the end of the polyene chain, in the vicinity of the nitrogen atom.[32] In particular, the $C_{14}{-}C_{15}$ bond is strongly reduced in length, indicating a partial penetration of the positive charge into the chain. Thus, our calculations are well in line with X-ray studies of iminium salts.

Studies of infinite conjugated chains using density functional theory have revealed limitations in the description of the dimerization amplitude, in the sense that the bond length alternation is underestimated.[56−58] A detailed analysis has shown that this effect can be traced back to deficiencies in the currently available exchange-correlation functionals.[59] However, previous density functional theory studies on several retinylidene iminium salts have already shown that the absolute bond lengths in the optimized structures are in overall agreement with X-ray crystallographic data, with a standard deviation of 0.03 Å.[60] Thus, although the dimerization amplitude is underestimated by the calculations, the reduction of the dimerization amplitude due to the delocalization of the positive charge in the protonated Schiff base tail is in agreement with the experiment.

According to recent double-quantum SSNMR data, the $C_{14}{-}C_{15}$ bond in the retinylidene chromophore of rhodopsin has a single bond character, and the excess charge is situated in the region $C_{12}{-}C_{13}$.[33] It should be noted that the error margin in the internuclear distances deduced from solid-state NMR measurements on the rhodopsin chromophore is of the same order as the aforementioned DFT calculations on the retinylidene iminium salts. The $C_{14}{-}C_{15}$ bond is estimated to be 1.428 Å with an uncertainty of 0.034 Å. Similarly, the $C_{13}{=}C_{14}$ bond is 1.368 Å, with an uncertainty of 0.027 Å.[33] A crucial factor that affects the bonding pattern scheme is the refined structure of the counterion and its exact position. Figure 3 shows that, with the counterion in the vicinity of the protonated Schiff base, the

TABLE 4: Normal Mode Vibrations of the 11-*cis*-Retinal PSB

freq [cm^{-1}]	normal mode description
	(a) In the Low-Frequency Region
105	$-0.138(C_{10}-C_{11}-C_{12}-C_{13}) - 0.129(C_{11}-C_{12}-C_{13}-C_{20}) + C_9$-methyl + β-ionone vibrations + lysine vibrations
122	$-0.148(C_8-C_9-C_{10}-C_{11}) - 0.193(C_9-C_{10}-C_{11}-C_{12}) - 0.257(C_{10}-C_{11}-C_{12}-C_{13}) + 0.104(C_{12}-C_{13}-C_{14}-C_{15}) - 0.228(C_{11}-C_{12}-C_{13}-C_{20}) + 0.170(C_{13}-C_{14}-C_{15}-N) - 0.307(C_9-C_{10}-C_{11}-H) - 0.172(C_{10}-C_{11}-C_{12}-H) + 0.205(C_{12}-C_{13}-C_{14}-H) + 0.222(C_{14}-C_{15}-N-H) + C_9$-methyl + C_{13}-methyl + lysine vibrations
172	$0.139(C_8-C_9-C_{10}-C_{11}) + 0.127(C_9-C_{10}-C_{11}-C_{12}) + 0.127(C_{10}-C_{11}-C_{12}-C_{13}) + 0.136(C_9-C_{10}-C_{11}-H) + 0.135(C_{10}-C_{11}-C_{12}-H) - 0.100(C_{13}-C_{14}-C_{15}-H) + C_9$-methyl + C_{13}-methyl + lysine vibrations
206	$-0.139(C_7-C_8-C_9-C_{10}) + 0.122(C_{10}-C_{11}-C_{12}-C_{13}) - 0.164(C_{12}-C_{13}-C_{14}-C_{15}) + 0.107(C_{11}-C_{12}-C_{13}-C_{20}) + 0.232(C_9-C_{10}-C_{11}-H) - 0.289(C_{12}-C_{13}-C_{14}-H) - 0.139(C_{13}-C_{14}-C_{15}-H) + 0.172(C_{14}-C_{15}-N-H) +$ β-ionone vibrations + lysine vibrations
341	$-0.161(C_5-C_6-C_7-C_8) + 0.323(C_7-C_8-C_9-C_{10}) + 0.103(C_8-C_9-C_{10}-C_{11}) - 0.242(C_9-C_{10}-C_{11}-C_{12}) - 0.108(C_{10}-C_{11}-C_{12}-C_{13}) - 0.100(C_{12}-C_{13}-C_{14}-C_{15}) + 0.253(C_8-C_9-C_{10}-H) - 0.167(C_{12}-C_{13}-C_{14}-H) +$ C_9-methyl + β-ionone vibrations
451	$-0.107(C_{10}-C_{11}-C_{12}) + 0.112(C_{14}-C_{15}-N) - 0.127(C_7-C_8-C_9-C_{10}) + 0.125(C_9-C_{10}-C_{11}-C_{12}) + 0.109(C_{10}-C_{11}-C_{12}-C_{13}) - 0.102(C_7-C_8-C_9-C_{19}) + C_{13}$-methyl + β-ionone vibrations
571	$0.165(C_7-C_8-C_9-C_{10}) - 0.200(C_9-C_{10}-C_{11}-C_{12}) - 0.153(C_{10}-C_{11}-C_{12}-C_{13}) + 0.113(C_7-C_8-C_9-C_{19}) + 0.300(C_8-C_9-C_{10}-H) - 0.130(C_9-C_{10}-C_{11}-H) + C_9$-methyl + β-ionone vibrations
587	$0.218(C_9-C_{10}-C_{11}-C_{12}) - 0.128(C_{10}-C_{11}-C_{12}-C_{13}) + 0.296(C_{12}-C_{13}-C_{14}-C_{15}) + 0.131(C_{13}-C_{14}-C_{15}-N) + 0.212(C_9-C_{10}-C_{11}-H) - 0.361(C_{10}-C_{11}-C_{12}-H) + 0.243(C_{14}-C_{15}-N-H) + C_9$-methyl + C_{13}-methyl + β-ionone vibrations
	(b) In the HOOP Region
829	$-0.118(C_{10}-C_{11}-C_{12}-C_{13}) + 0.171(C_{12}-C_{13}-C_{14}-C_{15}) - 0.241(C_{11}-C_{12}-C_{13}-C_{20}) + 0.318(C_9-C_{10}-C_{11}-H) + 0.571(C_{10}-C_{11}-C_{12}-H) - 0.293(C_{12}-C_{13}-C_{14}-H)$: assignment ($C_{11}H{=}C_{12}H$ B_2 HOOP) + $C_{14}H$ wag
851	$-0.166(C_9-C_{19}) + 0.165(C_{10}-C_{11}-C_{12}) - 0.115(C_{11}-C_{12}-C_{13}) + 0.137(C_7-C_8-C_9-C_{10}) + 0.115(C_{11}-C_{12}-C_{13}-C_{14}) + 0.113(C_5-C_6-C_7-H) + 0.130(C_6-C_7-C_8-H) + C_9$-methyl + β-ionone vibrations
875	$-0.203(C_7-C_8-C_9-C_{10}) - 0.235(C_6-C_7-C_8-H) + 0.440(C_8-C_9-C_{10}-H) + 0.193(C_{12}-C_{13}-C_{14}-H) +$ β-ionone vibrations: assignment $C_{10}H$ wag − C_8H wag
881	$-0.100(C_9-C_{19}) + 0.132(C_6-C_7-C_8) - 0.117(C_5-C_6-C_7-H) - 0.174(C_6-C_7-C_8-H) + 0.310(_{C8}-C_9-C_{10}-H) +$ β-ionone vibrations: assignment $C_{10}H$ wag
887	$0.116\ (C_6-C_7-C_8) + 0.101(C_{12}-C_{13}-C_{14}-C_{15}) - 0.261(C_5-C_6-C_7-H) - 0.257(C_6-C_7-C_8-H) - 0.231(C_8-C_9-C_{10}-H) - 0.180(C_9-C_{10}-C_{11}-H) - 0.190(C_{10}-C_{11}-C_{12}-H) - 0.361(C_{12}-C_{13}-C_{14}-H) - 0.157(C_{13}-C_{14}-C_{15}-H)$: assignment $C_{14}H$ wag + ($C_7H{=}C_8H$ B_g HOOP) + $C_{10}H$ wag
894	$0.194(C_5-C_6-C_7-H) + 0.333(C_8-C_9-C_{10}-H) - 0.100(C_{10}-C_{11}-C_{12}-H) - 0.188(C_{12}-C_{13}-C_{14}-H) - 0.115(C_{13}-C_{14}-C_{15}-H) + \beta$-ionone vibrations: assignment $C_{10}H$ wag
916	$-0.126(C_5-C_6-C_7-C_8) + 0.133(C_7-C_8-C_9-C_{10}) + 0.351(C_5-C_6-C_7-H) + 0.190(C_6-C_7-C_8-H) + 0.457(C_8-C_9-C_{10}-H) - 0.131(C_{13}-C_{14}-C_{15}-H) + C_9$-methyl + β-ionone vibrations: assignment $C_{10}H$ wag + C_7H wag
934	$-0.107(C_6-C_7-C_8-H) + \beta$-ionone vibrations
936	$-0.120(C_8-C_9-C_{10}-H) + 0.121(C_9-C_{10}-C_{11}-H) + 0.419(C_{12}-C_{13}-C_{14}-H) - 0.860(C_{13}-C_{14}-C_{15}-H) + 0.162(C_{14}-C_{15}-N-H)$: assignment ($C_{14}H{=}C_{15}H$ A_u HOOP)
954	$0.472(C_5-C_6-C_7-H) - 0.735(C_6-C_7-C_8-H) - 0.254(C_8-C_9-C_{10}-H) - 0.103(C_9-C_{10}-C_{11}-H) + \beta$-ionone vibrations: assignment ($C_7H{=}C_8H$ A_u HOOP) − $C_{10}H$ wag
975	$0.105(C_8-C_9-C_{10}-C_{11}) + 0.267(C_9-C_{10}-C_{11}-C_{12}) + 0.126(C_6-C_7-C_8-H) + 0.253(C_8-C_9-C_{10}-H) - 0.471(C_9-C_{10}-C_{11}-H) + 0.439(C_{10}-C_{11}-C_{12}-H) + 0.187(C_{12}-C_{13}-C_{14}-H) + C_9$-methyl: assignment ($C_{11}H{=}C_{12}H$ A_2 HOOP) − $C_{10}H$ wag
	(c) In the Fingerprint Region
1101	$0.120(C_{10}-C_{11}) + 0.121(C_{11}{=}C_{12}) + 0.101(C_6-C_7-C_8) - 0.141(C_9-C_{10}-C_{11}) - 0.157(C_{10}-C_{11}-C_{12}) + 0.170(C_{11}-C_{12}-H) - 0.156(C_8-C_9-C_{10}-C_{11}) - 0.140(C_8-C_9-C_{10}-H) + 0.104(C_{10}-C_{11}-C_{12}-H) + C_9$-methyl
1127	$-0.153(C_{14}-C_{15}-N-H) +$ lysine vibrations
1132	$0.172(C_6-C_7) + 0.176(C_6-C_7-H) + (C_6-C_7-C_8-C_9) + C_{13}$-methyl + β-ionone + lysine vibrations
1163	$0.107(C_6-C_7) - 0.108(C_6-C_7-C_8) + \beta$-ionone + lysine vibrations
1165	$0.133(C_{13}-C_{14}-H) + 0.194(C_{14}-C_{15}-H) + 0.155(C_{15}-N-H) + 0.132(C_{14}-C_{15}-N-H) +$ lysine vibrations
1191	$-0.115(C_6-C_7-H) + \beta$-ionone vibrations
1216	$-0.132(C_{12}-C_{13}) + 0.100(C_{13}{=}C_{14}) + 0.136(C_{10}-C_{11}-H) + 0.278(C_{11}-C_{12}-H) + 0.430(C_{13}-C_{14}-H) + 0.227(C_{14}-C_{15}-H) + 0.177(C_{15}-N-H) + 0.108(C_{12}-C_{13}-C_{14}-C_{15}) + 0.127(C_{12}-C_{13}-C_{14}-H) + C_{13}$-methyl
1231	$0.173(C_8-C_9) - 0.119(C_8-C_9-C_{10}) - 0.111(C_9-C_{10}-C_{11}) - 0.117(C_6-C_7-H) - 0.131(C_7-C_8-H) - 0.375(C_9-C_{10}-H) - 0.152(C_{10}-C_{11}-H) + 0.221(C_{11}-C_{12}-H) + 0.123(C_{13}-C_{14}-H) + 0.102(C_{14}-C_{15}-H) + 0.120(C_8-C_9-C_{10}-C_{11}) + 0.138(C_8-C_9-C_{10}-H) + C_9$-methyl
1241	$-0.423(C_6-C_7-H) - 0.122(C_7-C_8-H) + \beta$-ionone vibrations
1270	$-0.113(C_7{=}C_8) + 0.145(C_{14}-C_{15}) + 0.105(C_7-C_8-C_9) - 0.109(C_{13}-C_{14}-C_{15}) + 0.219(C_6-C_7-H) - 0.178(C_7-C_8-H) - 0.125(C_9-C_{10}-H) + 0.114(C_{10}-C_{11}-H) - 0.111(C_{11}-C_{12}-H) - 0.263(C_{13}-C_{14}-H) + 0.289(C_{14}-C_{15}-H) +$ β-ionone vibrations
1276	$-0.117(C_{14}-C_{15}-H) + \beta$-ionone vibrations
1286	$0.110(C_7{=}C_8) + 0.136(C_{14}-C_{15}) - 0.156(C_{13}-C_{14}-C_{15}) - 0.330(C_6-C_7-H) + 0.206(C_7-C_8-H) + 0.149(C_9-C_{10}-H) - 0.180(C_{13}-C_{14}-H) + 0.363(C_{14}-C_{15}-H) + \beta$-ionone vibrations + lysine vibrations
1292	$0.107(C_6-C_7) - 0.111(C_9{=}C_{10}) + 0.126(C_{10}-C_{11}) + 0.110(C_9-C_{19}) - 0.390(C_6-C_7-H) - 0.361(C_7-C_8-H) + 0.431(C_{10}-C_{11}-H) + 0.140(C_6-C_7-C_8-C_9) - 0.137(C_8-C_9-C_{10}-C_{11}) + 0.108(C_6-C_7-C_8-H) - 0.109(C_8-C_9-C_{10}-H) + \beta$-ionone vibrations

TABLE 4 (Continued)

freq [cm^{-1}]	normal mode description
	(d) In the Ethylenic Band
1478	$-0.131(C_{11}{=}C_{12}) - 0.118(C_6{-}C_7{-}H) + 0.261(C_{11}{-}C_{12}{-}H) - 0.176(C_{13}{-}C_{14}{-}H) + 0.364(C_{15}{-}N{-}H) + C_9$-methyl + lysine vibrations
1509	$0.120(C_5{=}C_6) - 0.137(C_6{-}C_7) + 0.199(C_7{=}C_8) - 0.135(C_8{-}C_9) + 0.113(C_{11}{=}C_{12}) + 0.117(C_{13}{=}C_{14}) + 0.266(C_6{-}C_7{-}H) - 0.402(C_7{-}C_8{-}H) - 0.225(C_9{-}C_{10}{-}H) + 0.238(C_{10}{-}C_{11}{-}H) - 0.171(C_{11}{-}C_{12}{-}H) - 0.152(C_{13}{-}C_{14}{-}H) + 0.130(C_{14}{-}C_{15}{-}H) + C_9$-methyl + C_{13}-methyl + β-ionone vibrations
1536	$-0.122(C_9{=}C_{10}) + 0.116(C_{11}{=}C_{12}) - 0.245(C_{12}{-}C_{13}) + 0.171(C_{13}{=}C_{14}) + 0.190(C_7{-}C_8{-}H) + 0.148(C_9{-}C_{10}{-}H) - 0.178(C_{10}{-}C_{11}{-}H) - 0.456(C_{11}{-}C_{12}{-}H) - 0.221(C_{13}{-}C_{14}{-}H) + 0.199(C_{15}{-}N{-}H) + C_9$-methyl + C_{13}-methyl
1557	$-0.132(C_5{=}C_6) - 0.112(C_6{-}C_7) + 0.137(C_7{=}C_8) - 0.137(C_9{=}C_{10}) + 0.249(C_{10}{-}C_{11}) - 0.182(C_{11}{=}C_{12}) + 0.135(C_6{-}C_7{-}H) - 0.209(C_7{-}C_8{-}H) + 0.420(C_9{-}C_{10}{-}H) - 0.487(C_{10}{-}C_{11}{-}H) - 0.127(C_{14}{-}C_{15}{-}H) + 0.116(C_{15}{-}N{-}H) + 0.112(C_{10}{-}C_{11}{-}C_{12}{-}C_{13}) + \beta$-ionone vibrations
1567	$-0.312(C_5{=}C_6) + 0.183(C_7{=}C_8) - 0.114(C_8{-}C_9) + 0.373(C_6{-}C_7{-}H) - 0.259(C_7{-}C_8{-}H) - 0.189(C_5{-}C_6{-}C_7{-}C_8) - 0.153(C_5{-}C_6{-}C_{7-H)} + \beta$-ionone vibrations
1622	$0.120(C_{13}{=}C_{14}) - 0.297(C_{14}{-}C_{15}) + 0.237(C_{15}{=}N) - 0.126(C_{10}{-}C_{11}{-}H) - 0.348(C_{13}{-}C_{14}{-}H) + 0.520(C_{14}{-}C_{15}{-}H) - 0.392(C_{15}{-}N{-}H)$

sign of the dimerization amplitude alternates between adjacent C−C polyene bonds, except in the terminal region toward the nitrogen atom. Without the counterion, the conjugation defect extends even further in the conjugated polyene chain; the sign alternation of the dimerization amplitude already ceases at C_{11}. A similar DFT study on the original Palczewski X-ray model structure with the counterion, where some constraints have been included in the calculation to mimic the tight binding pocket of the protein, reveals a less severe bond length perturbation than our present calculations.[61] Although there is still a significant reduction of the dimerization amplitude, no bond order inversion is observed at C_{13}. Earlier modeling studies also confirm that the bond length alternation pattern is sensitive to the counterion environment.[60] The most recent X-ray structure of rhodopsin revealed that several charged and/or polar amino acid residues are in close contact with the polyene chain of the ligand.[11] In particular, the glutamic acid residue Glu181 and the tyrosine residue Tyr268 are located in the vicinity of the $C_{10}{-}C_{13}$ region, and may therefore contribute in modulating the positive charge delocalization in the polyene. This is supported by site-directed mutagenesis studies of Glu181 or Tyr268, which lead to significant shifts in the spectral properties of the pigment.[62,63] In a recent study within an approximate DFT approach on a realistic model of the chromophore, in which the protein environment has been included explicitly, a slightly reduced bond length alternation pattern has been observed, with a considerable dimerization amplitude close to the Schiff base.[49] Thus, it can be inferred that the negative charge of the counterion in the rhodopsin protein is strongly delocalized in the region around the polyene chain of the chromophore; i.e., the results of the experimental and theoretical studies of the spatial ground-state structure of the rhodopsin chromophore converge toward a very soft counterion. This will modulate the delocalization of the positive charge and distort the conjugation effect that would otherwise be present due to the penetration of the positive charge into the polyene chain. The soft counterion prevents a bond order inversion at C_{13} in the rhodopsin chromophore.

Electronic Structure. Figure 4 presents the calculated and experimental ^{13}C isotropic chemical shifts of the neutral 11-*cis*-retinal SB.[64] As expected, the accuracy of the results is similar to the accuracy of previous ^{13}C NMR chemical shift calculations within the same level of theory on retinal isomers.[46] The rms error for the conjugated carbon atoms is 3.3 ppm, and the correlation coefficient is $\rho = 0.945$. Thus, it can be concluded that, for neutral retinylidene compounds, density functional theory provides ^{13}C NMR chemical shifts that are in near-quantitative agreement with the experiment. The calculated ^{13}C isotropic chemical shifts of the protonated models are shown in Figure 5, where they are compared with the experimental values obtained with ^{13}C solid-state MAS NMR studies of rhodopsin reconstituted with a uniformly ^{13}C-labeled retinal chromophore.[31] For the bare 11-*cis*-retinal PSB model, i.e., without a counterion near the protonated Schiff base, the rms error for the carbon atoms in the conjugated chain is 12.5 ppm, with a correlation coefficient $\rho = 0.660$. With a counterion in the vicinity of the protonated Schiff base, the results are appreciably different. The rms error reduces to 6.1 ppm, while the correlation coefficient between the experimental and calculated values increases to $\rho = 0.925$. The shielding estimates from the DFT calculations predict a C_{13} response downfield from the C_{15} signal, in line with the experiment.[16,23]

Previous comparison of the electron charge density distribution of the ground-state equilibrium structure of an 11-*cis*-retinal PSB + Cl^- model for the rhodopsin chromophore and the neutral 11-*cis*-retinal SB has revealed the presence of excess positive charge in the region near the protonated Schiff base.[26,27] This excess charge has been associated with a polaronic conjugation defect, which can transport charge along the conjugated chain in a molecular dynamics simulation. It can be instrumental in driving the isomerization of the chromophore.[26−29,65] In the ground state, the conjugation defect is stabilized by the electrostatic interaction between the polyene and the counterion. The extent of delocalization of the positive charge in the retinylidene chromophore of rhodopsin is correlated to the ^{13}C shifts measured for the carbon nuclei in the polyene chain.[66] The excess positive charge stabilized on the odd-numbered carbon atoms leads to increased shielding. This is accompanied by a concomitant upfield shift of the even-numbered carbon atoms, due to accumulation of negative charge on these atoms, induced by the positive charge on the odd-numbered carbon atoms via the Coulomb interaction. In the model without the counterion, the odd-numbered carbon atoms C_9 and C_{11} are shifted downfield, and the even-numbered carbon atoms C_{12} and C_{14} are shifted upfield relative to the model with the counterion included. This is in line with expectations. Including a counterion in the vicinity of the protonated nitrogen atom yields a less extended delocalization of the positive charge. This is consistent with the results of the spatial structure discussed in the previous section, where it was shown that the location of the center of the conjugation defect in the chromophore shifts closer to the nitrogen atom if the counterion is included in the model, while the positive charge is delocalized too far into the polyene chain if the counterion is not included. The double bonds are elongated and the single bonds are shortened due to the delocalization of the positive charge in the polyene chain. In the PSB model without the counterion,

TABLE 5: Normal Mode Vibrations of the 11-*cis*-Retinal PSB + CH_3COO^-

freq [cm^{-1}]		
calcd	exptl	normal mode description
		(a) In the Low-Frequency Region
276		$0.189(C_9-C_{10}-C_{11}-C_{12}) + 0.235(C_{10}-C_{11}-C_{12}-C_{13}) + 0.106(C_{11}-C_{12}-C_{13}-C_{14}) + 0.300(C_{11}-C_{12}-C_{13}-C_{20}) +$ $0.298(C_9-C_{10}-C_{11}-H) + 0.159(C_{10}-C_{11}-C_{12}-H) + 0.113(C_{14}-C_{15}-N-H) + C_9$-methyl + C_{13}-methyl + β-ionone vibrations + lysine vibrations
279		$-0.103(C_{10}-C_{11}-C_{12}-C_{13}) + 0.123(C_7-C_8-C_9-C_{19}) - 0.166(C_{11}-C_{12}-C_{13}-C_{20}) - 0.124(C_9-C_{10}-C_{11}-H) + C_9$-methyl + β-ionone vibrations
436		$0.175(C_7-C_8-C_9-C_{10}) - 0.229(C_9-C_{10}-C_{11}-C_{12}) - 0.128(C_{10}-C_{11}-C_{12}-C_{13}) - 0.180(C_9-C_{10}-C_{11}-H) + C_9$-methyl + C_{13}-methyl + β-ionone vibrations
536		$0.105(C_8-C_9-C_{10}) + 0.188(C_9-C_{10}-C_{11}-C_{12}) + 0.170(C_{10}-C_{11}-C_{12}-C_{13}) + 0.285(C_9-C_{10}-C_{11}-H) + C_{13}$-methyl + β-ionone vibrations
558		$-0.104(C_7-C_8-C_9-C_{10}) - 0.134(C_8-C_9-C_{10}-C_{11}) - 0.170(C_9-C_{10}-C_{11}-C_{12}) - 0.146(C_{10}-C_{11}-C_{12}-C_{13}) -$ $0.137(C_{11}-C_{12}-C_{13}-C_{14}) + 0.113(C_6-C_7-C_8-H) - 0.361(C_9-C_{10}-C_{11}-H) + 0.104(C_{10}-C_{11}-C_{12}-H) -$ $0.207(C_{12}-C_{13}-C_{14}-H) - 0.103(C_{13}-C_{14}-C_{15}-H) + C_{13}$-methyl + glutamate vibrations
		(b) In the HOOP Region[a]
947		$0.184(C_{12}-C_{13}-C_{14}-C_{15}) - 0.149(C_{11}-C_{12}-C_{13}-C_{20}) + 0.222(C_8-C_9-C_{10}-H) + 0.392(C_9-C_{10}-C_{11}-H) + 0.637(C_{10}-C_{11}-C_{12}-H) -$ $0.312(C_{12}-C_{13}-C_{14}-H) - 0.184(C_{13}-C_{14}-C_{15}-H) +$ lysine vibrations: assignment ($C_{11}H{=}C_{12}H$ B_2 HOOP) − $C_{14}H$ wag
954		$-0.150(C_7-C_8-C_9-C_{10}) - 0.112(C_{12}-C_{13}-C_{14}-C_{15}) - 0.211(C_5-C_6-C_7-H) - 0.229(C_6-C_7-C_8-H) +$ $0.501(C_8-C_9-C_{10}-H) + 0.203(C_9-C_{10}-C_{11}-H) + 0.162(C_{10}-C_{11}-C_{12}-H) + 0.394(C_{12}-C_{13}-C_{14}-H) +$ $0.326(C_{13}-C_{14}-C_{15}-H) +$ lysine vibrations + β-ionone vibrations: assignment $C_{10}H$ wag + ($C_{14}H-C_{15}H$ B_g HOOP) − ($C_7H{=}C_8H$ B_g HOOP) + ($C_{11}H{=}C_{12}H$ B_2 HOOP)
976		$0.117(C_7-C_8-C_9-C_{10}) + 0.369(C_5-C_6-C_7-H) + 0.224(C_6-C_7-C_8-H) - 0.270(C_8-C_9-C_{10}-H) + 0.234(C_9-C_{10}-C_{11}-H) +$ $0.315(C_{10}-C_{11}-C_{12}-H) + 0.304(C_{12}-C_{13}-C_{14}-H) + 0.271(C_{13}-C_{14}-C_{15}-H) +$ lysine vibrations + β-ionone vibrations: assignment ($C_7H{=}C_8H$ B_g HOOP) + ($C_{11}H{=}C_{12}H$ B_2 HOOP) + ($C_{14}H-C_{15}H$ B_g HOOP) − $C_{10}H$ wag
982		$0.315(C_8-C_9-C_{10}-H) - 0.115(C_{10}-C_{11}-C_{12}-H) + \beta$-ionone vibrations: assignment $C_{10}H$ wag
993	843	$0.449(C_5-C_6-C_7-H) + 0.205(C_6-C_7-C_8-H) + 0.615(C_8-C_9-C_{10}-H) - 0.132(C_{10}-C_{11}-C_{12}-H) + \beta$-ionone vibrations: assignment $C_{10}H$ wag + ($C_7H{=}C_8H$ B_g HOOP)
998		$0.117(C_5-C_6-C_7-H) + \beta$-ionone vibrations
1019		$0.158(C_9-C_{10}-C_{11}-H) + 0.488(C_{12}-C_{13}-C_{14}-H) - 0.817(C_{13}-C_{14}-C_{15}-H) - 0.125(C_{14}-C_{15}-N-H) + C_{13}$-methyl + glutamate vibrations: assignment ($C_{14}H-C_{15}H$ A_u HOOP)
1027		$0.192(C_{12}-C_{13}-C_{14}-H) - 0.270(C_{13}-C_{14}-C_{15}-H) +$ glutamate vibrations
1035		$0.231(C_6-C_7-C_8-H) + 0.105(C_8-C_9-C_{10}-H) + C_{13}$-methyl + β-ionone vibrations
1040		$-0.146(C_8-C_9-C_{10}-H) + 0.202(C_9-C_{10}-C_{11}-H) - 0.175(C_{12}-C_{13}-C_{14}-H) + C_{13}$-methyl + glutamate + β-ionone vibrations
1047		$0.191(C_5-C_6-C_7-H) - 0.585(C_6-C_7-C_8-H) + C_{13}$-methyl + β-ionone vibrations
1053	976	$-0.510(C_5-C_6-C_7-H) + 0.557(C_6-C_7-C_8-H) + C_{13}$-methyl + C_{13}-methyl + β-ionone vibrations: assignment ($C_7H{=}C_8H$ A_u HOOP)
1056	970	$-0.164(C_9-C_{10}-C_{11}-C_{12}) - 0.198(C_8-C_9-C_{10}-H) + 0.439(C_9-C_{10}-C_{11}-H) - 0.360(C_{10}-C_{11}-C_{12}-H) - 0.148(C_{12}-C_{13}-C_{14}-H) +$ C_{13}-methyl + C_{13}-methyl + lysine vibrations: assignment ($C_{11}H{=}C_{12}H$ A_2 HOOP)
		(c) In the Fingerprint Region[b]
1128	1098	$0.140(C_{10}-C_{11}) + 0.103(C_{11}{=}C_{12}) - 0.143(C_9-C_{10}-C_{11}) - 0.165(C_{10}-C_{11}-C_{12}) - 0.148(C_8-C_9-C_{10}-C_{11}) -$ $0.157(C_8-C_9-C_{10}-H) + 0.147(C_{10}-C_{11}-C_{12}-H) + C_9$-methyl + C_{13}-methyl
1155		$-0.217(C_6-C_7) + 0.108(C_6-C_7-C_8) + 0.102(C_7-C_8-C_9) - 0.135(C_6-C_7-H) - 0.123(C_6-C_7-C_8-C_9) + C_{13}$-methyl + β-ionone vibrations
1188		$-0.167(C_{14}-C_{15}-N-H) +$ lysine vibrations
1197		$-0.126(C_{15}-N-H) - 0.102(C_{14}-C_{15}-N-H) +$ lysine vibrations
1239	1239	$-0.140\ (C_{12}-C_{13}) + 0.204(C_{10}-C_{11}-H) + 0.162(C_{11}-C_{12}-H) - 0.446(C_{13}-C_{14}-H) + 0.136(C_{14}-C_{15}-H) + 0.166(C_{15}-N-H) -$ $0.130(C_8-C_9-C_{10}-C_{11}) + 0.103(C_{12}-C_{13}-C_{14}-C_{15}) - 0.124(C_8-C_9-C_{10}-H) + C_9$-methyl + C_{13}-methyl + lysine vibrations
1262	1217	$-0.200(C_8-C_9) + 0.140(C_9-C_{19}) + 0.101(C_7-C_8-C_9) + 0.181(C_8-C_9-C_{10}) + 0.171(C_9-C_{10}-C_{11}) + 0.243(C_9-C_{10}-H) -$ $0.176(C_{11}-C_{12}-H) - 0.178(C_{13}-C_{14}-H) - 0.102(C_{14}-C_{15}-H) - 0.126(C_8-C_9-C_{10}-C_{11}) - 0.110(C_8-C_9-C_{10}-H) +$ C_9-methyl + β-ionone vibrations
1279		$-0.203(C_6-C_7-H) + 0.148(C_7-C_8-H) - 0.108(C_9-C_{10}-H) + \beta$-ionone vibrations
1285	1190	$-0.185(C_{14}-C_{15}) + 0.164(C_{13}-C_{14}-C_{15}) - 0.212(C_{14}-C_{15}-N) - 0.132(C10-C_{11}-H) + 0.384(C_{13}-C_{14}-H) -$ $0.328(C_{14}-C_{15}-H) - 0.140(C_{12}-C_{13}-C_{14}-H) +$ lysine vibrations
1307	1270	$0.140(C_{10}-C_{11}) + 0.110(C_{13}-C_{20}) + 0.144(C_{11}-C_{12}-C_{13}) + 0.184(C_{12}-C_{13}-C_{14}) + 0.179(C_{13}-C_{14}-C_{15}) + 0.128(C_{14}-C_{15}-N) -$ $0.285(C_7-C_8-H) + 0.445(C_{10}-C_{11}-H) - 0.201(C_{11}-C_{12}-H) - 0.148(C_{13}-C_{14}-H) - 0.181(C_{14}-C_{15}-H) + C_9$-methyl + lysine vibrations
1315		$0.104(C_8-C_9) - 0.108(C_9-C_{19}) + 0.495(C_6-C_7-H) + 0.416(C_7-C_8-H) + 0.101(C_9-C_{10}-H) - 0.121(C_6-C_7-C_8-C_9) -$ $0.101(C_6-C_7-C_8-H) + \beta$-ionone vibrations
		(d) In the Ethylenic Band[c]
1503		$-0.120(C_{11}{=}C_{12}) - 0.132(C_6-C_7-H) + 0.121(C_{11}-C_{12}-H) - 0.166(C_{13}-C_{14}-H) + 0.384(C_{15}-N-H) + C_9$-methyl + C_{13}-methyl + lysine vibrations
1518		glutamate vibrations
1554		$0.123(C_9{=}C_{10}) - 0.118(C_{11}{=}C_{12}) + 0.231(C_{12}-C_{13}) - 0.161(C_{13}{=}C_{14}) - 0.168(C_{12}-C_{13}-C_{20}) - 0.178(C_6-C_7-H) + 0.102(C_7-C_8-H) -$ $0.199(C_9-C_{10}-H) + 0.189(C_{10}-C_{11}-H) + 0.517(C_{11}-C_{12}-H) + 0.180(C_{13}-C_{14}-H) - 0.106(C_{15}-N-H) + C_9$-methyl + C_{13}-methyl
1561	1548	$-0.105(C_6-C_7) + 0.196(C_7{=}C_8) - 0.154(C_8-C_9) + 0.199(C_9{=}C_{10}) - 0.180(C_{10}-C_{11}) - 0.153(C_{11}{=}C_{12}) + 0.156(C_8-C_9-C_{19}) +$ $0.256(C_6-C_7-H) - 0.336(C_7-C_8-H) - 0.390(C_9-C_{10}-H) + 0.411(C_{10}-C_{11}-H) + C_9$-methyl
1585		$0.135(C_6-C_7) - 0.256(C_7{=}C_8) + 0.129(C_8-C_9) - 0.159(C_{10}-C_{11}) + 0.205(C_{11}{=}C_{12}) - 0.126(C_{12}-C_{13}) + 0.101(C_{12}-C_{13}-C_{20}) -$ $0.346(C_6-C_7-H) + 0.358(C_7-C_8-H) - 0.257(C_9-C_{10}-H) + 0.306(C_{10}-C_{11}-H) - 0.209(C_{11}-C_{12}-H) -$ $0.115(C_{10}-C_{11}-C_{12}-C_{13}) + C_{13}$-methyl
1616		$0.379(C_5{=}C_6) - 0.107(C_6-C_7) - 0.203(C_6-C_7-H) + 0.230(C_5-C_6-C_7-C_8) + 0.230(C_5-C_6-C_7-H) + \beta$-ionone vibrations
1639	1653	$0.133(C_{13}{=}C_{14}) - 0.298(C_{14}-C_{15}) + 0.231(C_{15}{=}N) - 0.351(C_{13}-C_{14}-H) + 0.557(C_{14}-C_{15}-H) - 0.410(C_{15}-N-H) +$ C_{13}-methyl + lysine vibrations

[a] Experimental values from refs 20 and 22. [b] Experimental values from ref 21. [c] Experimental values from ref 22.

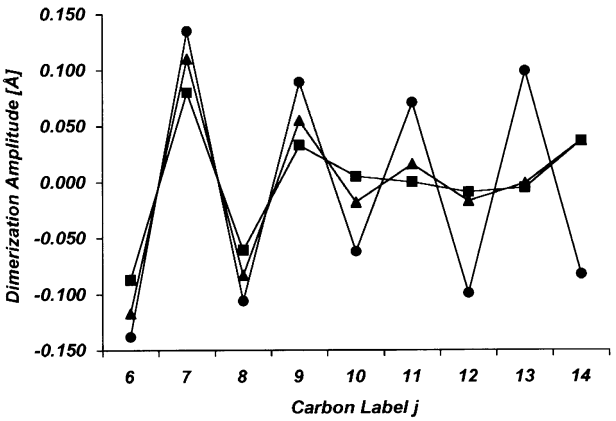

Figure 3. Calculated dimerization amplitudes for the conjugated polyene chain of the neutral 11-*cis*-retinal SB (●), the 11-*cis*-retinal PSB (■) and the 11-*cis*-retinal PSB + CH_3COO^- (▲) model compounds.

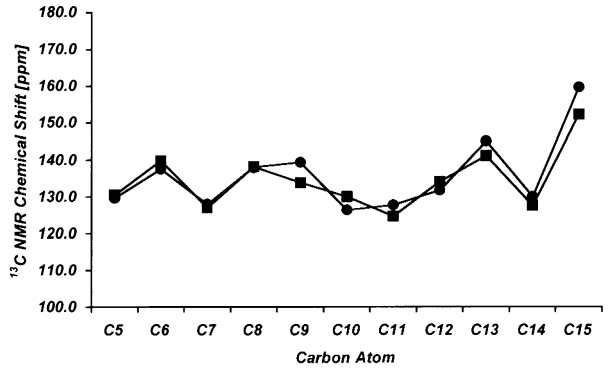

Figure 4. Calculated (■) and experimental ((●) from ref 64) ^{13}C NMR chemical shift in the conjugated backbone chain of the 11-*cis*-retinal SB.

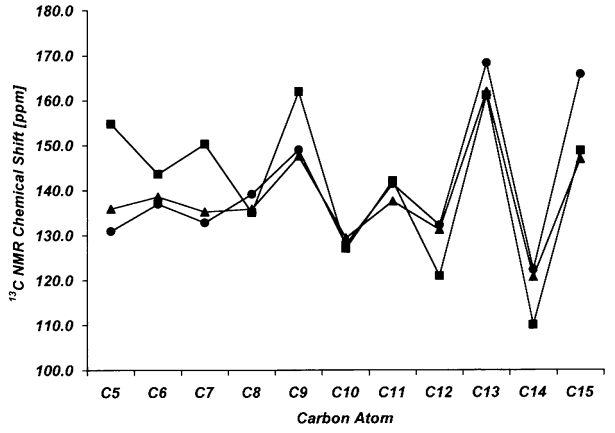

Figure 5. Calculated ^{13}C NMR chemical shift in the conjugated backbone chain of the 11-*cis*-retinal PSB (■) and the 11-*cis*-retinal PSB + CH_3COO^- (▲) model compounds compared with the experimental ^{13}C solid-state NMR chemical shifts in the retinylidene chromophore of rhodopsin ((●) from ref 31). All values are reported relative to TMS.

the bond length alternation pattern is disturbed in the region C_9-C_{15}. Including the counterion stabilizes this perturbation in the region $C_{12}-C_{15}$. The solid-state NMR results, however, suggest an additional effect that is not reproduced by our calculations.[33] The bond length perturbation is found mainly at $C_{12}-C_{13}$, while the region near the Schiff base appears to be less perturbed. Thus, a distortion of the conjugation defect is observed. Such a distortion can be attributed to additional

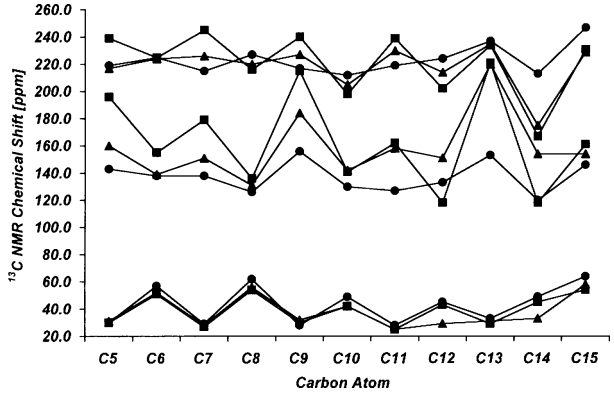

Figure 6. Calculated principal Cartesian components of the ^{13}C NMR chemical shift tensor in the conjugated backbone chain of the neutral 11-*cis*-retinal SB (●), the 11-*cis*-retinal PSB (■), and the 11-*cis*-retinal PSB + CH_3COO^- (▲) model compounds. All values are reported relative to TMS.

electrostatic interaction with polar amino acid residues in the surrounding protein pocket, resulting in a complex counterion in which the negative charge is strongly delocalized. This supports the conclusions inferred from our calculations of the ground-state spatial structure discussed in the previous section, where such a soft counterion has been suggested to explain the difference between the spatial characteristics obtained by experimental studies on rhodopsin and theoretical studies on protonated Schiff base model compounds.

For both our model compounds, the calculated ^{13}C chemical shift values of C_{15} exhibit a large deviation from the experimental value in the upfield direction. However, in this case an explanation in terms of a different position or type of counterion for the rhodopsin chromophore is unlikely. Similar results have been obtained in chemical shift calculations on high-resolution X-ray structures of retinylidene iminium salts for which the geometry and the type and position of the counterion are known precisely.[60] Hence, this discrepancy is systematic. It is likely that the deviations from experiment are due to the poor description of the polarizability of long conjugated chains by the commonly used exchange-correlation functionals.[67]

In Figure 6, the calculated principal Cartesian components of the ^{13}C chemical shift tensor in the conjugated chain of our model compounds are compared. The π-electron perturbations due to protonation of the Schiff base primarily affect the in-plane components of the chemical shift tensor, i.e., δ_{11} and δ_{22}.[65] The δ_{22} components of the odd numbered carbon atoms in the conjugated chain shift significantly downfield upon protonation of the Schiff base. The δ_{22} components of the even numbered carbon atoms show a similar effect, i.e., they are shifted downfield, but are significantly less sensitive to the excess charge. The largest component of the chemical shift tensor, δ_{11}, is affected for all carbon atoms in the conjugated chain upon protonation of the Schiff base. For the odd numbered carbon atoms, this component exhibits a downfield shift, whereas for the even numbered carbon atoms this component shows an upfield shift. Both in-plane components show an increased odd−even effect due to the positive charge in the polyene chain.

Vibrational Structure. An important feature of the resonance Raman spectrum of rhodopsin is the $C_{15}=N$ stretch peak in the ethylenic band. For the neutral 11-*cis*-retinal SB, our calculations predict this stretch to appear at 1635 cm^{-1} where it mixes with the $C_{13}=C_{14}$ and $C_{14}-C_{15}$ stretches. In addition, contributions from the $C_{14}H$ and $C_{15}H$ in-plane rocks are found theoretically. The calculated frequency is in perfect agreement with the experimental value detected at 1632 cm^{-1}.[55] According to the

ab initio calculations on the 11-*cis*-retinal PSB + CH_3COO^- model, the C_{15}═N stretch character in the ethylenic band is mainly found at 1639 cm^{-1}, where it is coupled with the C_{14}—C_{15} stretch to form an asymmetric (C_{14}—C_{15}═N) stretching vibration. The local mode decomposition given in Table 5c reveals that this normal mode has a strong contribution from the C_{13}═C_{14} stretch coordinate and the C_{14}H, C_{15}H, and NH in-plane rocks. For our 11-*cis*-retinal PSB model without the counterion, a similar vibrational mode is predicted at 1622 cm^{-1}. The coupling of the C_{14}—C_{15} stretch and the C_{15}═N stretch is only found in the protonated chromophores and results from the conjugation defect in the Schiff base tail, which causes a strong decrease in C_{15}═N bond order, accompanied by a concomitant increase in the C_{14}—C_{15} bond order. Consequently, the intrinsic frequencies of the C_{15}═N and C_{14}—C_{15} stretch coordinates approach each other in the PSB relative to the SB, which increases their mutual coupling.[68] In contrast, in the experimental resonance Raman spectrum of rhodopsin, the small peak observed at 1654 cm^{-1} has been assigned to the C_{15}═N stretch, based on the downshift of this mode to 1623 cm^{-1} upon N-deuteration.[20,21] This suggests that the C_{15}═N has a strong double bond character.

The frequency of the (C_{14}—C_{15}═N) asymmetric stretch resulting from our calculations is higher for the model with the counterion than for the model without the counterion; i.e., the frequency of the C_{15}═N stretch is sensitive to the counterion environment. The mutual coupling of the C_{15}═N and C_{14}—C_{15} stretch coordinates is stronger in the 11-*cis*-retinal PSB model without the counterion than for the PSB model with the counterion, and as a result, the frequency of the resulting (C_{14}—C_{15}═N) asymmetric stretch is lower than that of the corresponding normal mode in the 11-*cis*-retinal PSB + CH_3COO^- model. The much higher C_{15}═N stretch frequency observed for rhodopsin can be ascribed to additional electrostatic interactions with several charged and/or polar amino acid residues in the neighborhood of the polyene chain of the ligand, in accordance with the recently obtained X-ray structure.[11] This would distort the polaronic conjugation defect in the chromophore and prevent the coupling of the C_{14}—C_{15} and C_{15}═N stretch coordinates. Further tuning of the frequency can be achieved by including one or several water molecules in our model in the vicinity of the Schiff base proton and the acetate ion. Due to the hydrogen-bonded network thus formed, the center of the conjugation defect would be located closer to the nitrogen atom, and consequently, the frequency of the C_{15}═N stretching mode can be expected to shift to a higher value. There is compelling evidence from ^{15}N MAS NMR experiments for such a hydrogen-bonded network.[15]

The C—C single bond stretches represent the most characteristic part of the vibrational spectrum and form the fingerprint region in the range 1000—1400 cm^{-1}. In polyenes, these stretches are strongly coupled, because they interact via the π backbone electrons. In retinylidene compounds, the local character of the vibrations is attributed to the asymmetry imposed by the side methyl groups bound to C_9 and C_{13} of the conjugated backbone chain, which decouples the backbone modes.[69] The delocalization of the local mode vibrations revealed by the density functional theory calculations and presented in Tables 3b, 4b, and 5b, i.e., for the neutral as well as the protonated model compounds, challenges this assumption, since it is obvious that several local mode coordinates contribute to any normal mode. The assignments of the peaks in the resonance Raman spectrum of rhodopsin in terms of local coordinates have been based on a normal-mode analysis of retinal PSBs performed with the QCFF-p program, using a modified Urey—Bradley force field.[70] A rigorous force field analysis has been performed on all-*trans*-retinal, its protonated Schiff base, and bacteriorhodopsin.[71,72] The force constants resulting from these analyses provide an indication of an enhanced double bond character of the C_{14}—C_{15} bond for the retinylidene chromophore in bacteriorhodopsin. The force constant of the C_{14}—C_{15} bond, K(14—15), in all-*trans*-retinal is 3.13 mdyn/Å. In the all-*trans*-retinal PSB, K(14—15) increases to a value of 4.01 mdyn/Å.[71] This increase can be attributed to two effects. First, the Schiff base nitrogen is less electronegative than the oxygen atom in the aldehyde. This results in a weaker affinity for the electrons in the adjacent C_{14}—C_{15} bond, and therefore in an increased C_{14}—C_{15} bond order. Second, the delocalization of the positive charge increases the C_{14}—C_{15} bond order. In bacteriorhodopsin, the force constant K(14—15) further increases to 4.21 mdyn/Å.[72] In both the all-*trans*-retinal PSB and bacteriorhodopsin, the force constant of the C_{14}—C_{15} bond is larger than the force constant of the C_8—C_9 bond. The C_8—C_9 local mode stretches of these compounds, however, appear at a higher frequency than the C_{14}—C_{15} local mode stretches. This supports the conclusion that local bond orders cannot be assessed from frequencies detected with resonance Raman spectroscopy based on local mode assignments only.

The vibrational frequencies of the normal modes in the fingerprint region of the neutral 11-*cis*-retinal SB predicted by our density functional theory calculations, presented in Table 3b, are in excellent agreement with the experimental values. The C_{14}—C_{15} stretch character is found mainly at 1155 cm^{-1}, which is in good agreement with the experimental value of 1157 cm^{-1}.[21] The 11-*cis*-retinal PSB + CH_3COO^- model reveals C_{14}—C_{15} stretch character in the normal mode at 1285 cm^{-1} in the fingerprint region, where it mixes with the C_{14}H and C_{15}H in-plane rocking vibrations. The upshift of the frequency of the normal mode containing C_{14}—C_{15} stretch character is a consequence of the delocalization of the positive charge introduced in the chromophore by protonation of the Schiff base nitrogen atom. Due to the charge delocalization, the bond order of the C_{14}—C_{15} increases, and therefore, its intrinsic stretching frequency increases. For rhodopsin, the C_{14}—C_{15} stretch has been detected primarily at 1190 cm^{-1}, i.e., at a higher frequency than for the neutral 11-*cis*-retinal SB, in accordance with our theoretical findings. However, the increase in frequency calculated for the 11-*cis*-retinal PSB + CH_3COO^- model is much larger, indicating that the C_{14}—C_{15} bond in our model has much more enhanced double bond character than the C_{14}—C_{15} bond in the chromophore of rhodopsin. This reinforces our findings from the previous section, where it has been inferred that in rhodopsin a complex counterion with a strongly delocalized negative charge distorts the conjugation defect in the Schiff base region.

A conjugation defect in the Schiff base region does affects the vibrational spectrum not only in the ethylenic band and the fingerprint region, but also in the HOOP region. Wags of *trans* ethylenic protons couple strongly across a double bond to form A_u and B_g symmetry combinations.[69] The in-phase combination, in which both protons move out of the plane in the same direction, is designated the A_u HOOP mode, while the out-of-phase combination, in which the protons move out of plane in opposite directions, is designated the B_g HOOP mode. The values for the A_u HOOP mode and the B_g HOOP mode are separated by ~150 cm^{-1}, with the A_u HOOP mode at the higher wavenumber. The A_u HOOP modes are very characteristic in IR spectra but usually appear weakly or not at all in resonance

Raman spectra. A vibration can only be Raman active if it gives rise to a change in the polarizability of the molecule.[73] This change in polarizabilty leads to an induced dipole through interaction with the electric field of the incident laser radiation. Due to their symmetry, the A_u HOOP modes in general do not induce a change in the polarizabilty of a molecule. A relative distortion of the planar geometry in either the ground state or the resonant excited state, however, can cause these modes to appear strongly in the resonance Raman spectrum. The B_g HOOP mode is expected to be weak in both IR and Raman spectra.

In the HOOP region, the density functional theory normal mode calculations on the 11-*cis*-retinal PSB + CH_3COO^- model reveal a $C_{14}H-C_{15}H$ A_u HOOP mode at 1019 cm^{-1}. The coupling of the $C_{14}H$ and $C_{15}H$ wags is a direct result of the enhanced double bond character of the $C_{14}-C_{15}$ bond, due to the conjugation defect in the Schiff base region. In the neutral 11-*cis*-retinal SB, the $C_{14}H$ and $C_{15}H$ are found to be uncoupled. The $C_{14}H$ wag is calculated at 927 cm^{-1} and the $C_{15}H$ wag at 985 cm^{-1}. In the chromophore of rhodopsin, the $C_{14}H$ and $C_{15}H$ wags are not expected to couple, because the $C_{14}-C_{15}$ bond does not have an enhanced double bond character. The enhanced double bond character of the $C_{14}-C_{15}$ bond is present, however, in retinylidene iminium salts, as evidenced by X-ray crystallography.[32] Because the retinylidene iminium salts are essentially planar in the Schiff base region, the $C_{14}H-C_{15}H$ A_u HOOP mode is not expected to appear in the resonance Raman spectra. This normal mode should in principle be detectable, however, by means of FTIR spectroscopy on deuterated retinylidene iminium salts. We therefore suggest further experimental investigations in the bond order of the $C_{14}-C_{15}$ bond in these compounds by means of FTIR spectroscopy.

Conclusions

On the basis of density functional theory studies, a comprehensive picture is presented of the spatial, electronic, and vibrational structure of neutral and protonated 11-*cis*-retinal Schiff base models. For the neutral Schiff base model, a convergent and comprehensive model picture emerges, which is consistent with the available experimental results from ^{13}C NMR and resonance Raman spectroscopy. The calculated ^{13}C NMR chemical shifts in the conjugated chain of the neutral Schiff base model are in near-quantitative agreement with experiment. The calculated vibrational frequencies are in very good agreement with the experimental data. We conclude that, in principle, density functional theory is a very useful tool in the prediction of vibrational modes and the interpretation of experimentally obtained NMR and Raman spectra.

For the protonated models, the calculations reveal a polaronic conjugation defect in the ground state in the Schiff base region. Consequently, the $C_{14}-C_{15}$ bond has enhanced double bond character, while the $C_{13}=C_{14}$ and $C_{15}=N$ bonds have reduced double bond character. This phenomenon affects the vibrational structure in an extended region of the spectrum. The C−C, C=C, and C=N stretches in the fingerprint region and the ethylenic band are significantly delocalized; i.e., several components contribute to a normal mode vibration. This implies that it is difficult to assess local bond orders from the observed frequencies via a direct local mode assignment only. According to the ab initio calculations, the conjugation defect expresses itself in a coupling of the $C_{14}-C_{15}$ and $C_{15}=N$ stretching coordinates. This results in an asymmetric ($C_{14}-C_{15}=N$) stretch component in the ethylenic band at 1639 cm^{-1}. In addition, the calculations reveal a strong coupling of the $C_{14}H$ and $C_{15}H$ wags due to the presence of the conjugation defect: a coupled $C_{14}H-C_{15}H$ A_u HOOP mode appears at 1019 cm^{-1} in the calculated vibrational spectrum of the model compound. In principle, such a coupling can be detected by means of FTIR spectroscopic measurements on 14-D, 15-D, and 14,15-D_2 derivatives of the compound. It would be interesting to perform such measurements on retinylidene iminium salts for which evidence has been found for an enhanced double bond character of the $C_{14}-C_{15}$ bond by means of X-ray crystallography.[32] This would provide additional experimental support for the essential difference between the bonding pattern schemes of the model compounds and the chromophore in rhodopsin.

Like the normal mode vibrations, the calculated ^{13}C shifts in the polyene chain are also correlated with perturbations of the bond length alternation pattern. The protonated models show a C_{13} response that is more deshielded than that of C_{15}, supporting the presence of a polaronic charge effect in the protonated Schiff base and an accumulation of charge at C_{13}. This is in line with NMR spectroscopic data obtained for protonated Schiff base model compounds as well as for the retinylidene chromophore of rhodopsin. However, the bonding pattern scheme in the conjugated chain is also very sensitive to the counterion environment. The bond order switch at C_{13} as calculated for our model compounds is not in line with the experimental data of rhodopsin. It can therefore be inferred that the negative charge of the counterion in the rhodopsin protein is strongly delocalized in the region around the polyene chain of the chromophore. This soft counterion modulates the delocalization of the positive charge and distorts the conjugation effect that would otherwise be present due to the penetration of the positive charge into the polyene chain: i.e., it prevents a bond order inversion at C_{13} and provides a way for the excess charge to hop over the Schiff base region.

Finally, it transpires that both for the optical spectroscopy and the NMR a description in terms of molecular properties at a length scale approaching the size of the ligand is necessary to arrive at a converging picture, to keep track of the correlations between the various sites in the electronic structure and the bonds in the vibrational structure. Thus, in the interpretation of NMR results, a polaronic picture is preferred over a description in terms of individual atomic charge densities. Likewise, a normal mode interpretation is preferred over a local mode assignment for the description of the vibrational structure.

Acknowledgment. We are very grateful to Walter Frizzera who provided the graphical software used to visualize the vibrational modes of the calculations. We thank Marc van Hemert for providing the software to calculate the transformation of the normal mode vibrations from Cartesian to internal coordinates. Johan Lugtenburg is acknowledged for encouraging this project and for stimulating discussions. This work was financially supported by the PIONIER program of The Netherlands Organization for Scientific Research (NWO).

References and Notes

(1) Wald, G. *Science* **1968**, *162*, 230−239.
(2) Schoenlein, R. W.; Peteanu, L. A.; Mathies, R. A.; Shank, C. V. *Science* **1991**, *254*, 412−415.
(3) Birge, R. R.; Einters, C. M.; Knapp, H. M.; Murray, L. P. *Biophys. J.* **1988**, *53*, 367−385.
(4) Cooper, A. *Nature* **1979**, *282*, 531−533.
(5) Schick, G. A.; Cooper, T. M.; Holloway, R. A.; Murray, L. P.; Birge, R. R. *Biochemistry* **1987**, *26*, 2556−2562.
(6) Stryer, L. *Sci. Am.* **1987**, *257*, 32−40.
(7) Birge, R. R. *Biochim. Biophys. Acta* **1990**, *1016*, 293−327.
(8) Han, M.; Smith, S. O. *Biochemistry* **1995**, *34*, 1425−1432.

(9) Palczewski, K.; Kumasaka, T.; Hore, T.; Behnke, C. A.; Motoshima, H.; Fox, B. A.; Le Trong, I.; Teller, D. C.; Okada, T.; Stenkamp, R. E.; Yamamoto, M.; Miyano, M. *Science* **2000**, *289*, 739−745.
(10) Teller, D. C.; Okada, T.; Behnke, C. A.; Palczewski, K.; Stenkamp, R. E. *Biochemistry* **2002**, *40*, 7761−7772.
(11) Okada, T.; Fujoyoshi, Y.; Silow, M.; Navarro, J.; Landau, E. M.; Schchida, Y. *Proc. Natl. Acad. Sci. U.S.A.* **2002**, *99*, 5982−5987.
(12) Nathans, J. *Biochemistry* **1990**, *29*, 9746−9752.
(13) Zhukovsky, E. A.; Oprian, D. D. *Science* **1989**, *246*, 928−930.
(14) Sakmar, T. P.; Franke, R. R.; Khorana, H. G. *Proc. Natl. Acad. Sci. U.S.A.* **1989**, *86*, 8309−8313.
(15) Creemers, A. F. L.; Klaassen, C. H. W.; Bovee-Geurts, P. H. M.; Kelle, R.; Kragl, U.; Raap, J.; de Grip, W. J.; Lugtenburg, J.; de Groot, H. J. M. *Biochemistry* **1999**, *38*, 7195−7199.
(16) Smith, S. O.; Palings, I.; Miley, M. E.; Courtin, J.; de Groot, H.; Lugtenburg, J.; Mathies, R. A.; Griffin, R. G. *Biochemistry* **1990**, *29*, 8158−8164.
(17) Verdegem, P. J. E.; Bovee-Geurts, P. H. M.; de Grip, W. J.; Lugtenburg, J.; de Groot, H. J. M. *Biochemistry* **1999**, *38*, 11316−11324.
(18) Feng, X.; Verdegem, P. J. E.; Lee, Y. K.; Sandström, D.; Edén, M.; Bovee-Geurts, P.; de Grip, W. J.; Lugtenburg, J.; de Groot, H. J. M.; Levitt, M. H. *J. Am. Chem. Soc.* **1997**, *119*, 6853−6857.
(19) Feng, X.; Verdegem, P. J. E.; Edén, M.; Sandström, D.; Lee, Y. K.; Bovee-Geurts, P. H. M.; de Grip, W. J.; Lugtenburg, J.; de Groot, H. J. M.; Levitt, M. H. *J. Biomol. NMR* **2000**, *16*, 1−8.
(20) Eyring, G.; Curry, B.; Broek, A.; Lugtenburg, J.; Mathies, R. A. *Biochemistry* **1982**, *21*, 384−394.
(21) Palings, I.; Pardoen, J. A.; van den Berg, E.; Winkel, C.; Lugtenburg, J.; Mathies, R. A. *Biochemistry* **1987**, *26*, 2544−2556.
(22) Lin, S. W.; Groesbeek, M.; van der Hoef, I.; Verdegem, P.; Lugtenburg, J.; Mathies, R. A. *J. Phys. Chem. B* **1998**, *102*, 2787−2806.
(23) Verhoeven, M. A.; Creemers, A. F. L.; Bovee-Geurts, P. H. M.; de Grip, W. J.; Lugtenburg, J.; de Groot, H. J. M. *Biochemistry* **2001**, *40*, 3282−3288.
(24) Car, R.; Parrinello, M. *Phys. Rev. Lett.* **1985**, *55*, 2471−2474.
(25) Pastore, G.; Smargiassi, E.; Buda, F. *Phys. Rev. A* **1991**, *44*, 6334−6347.
(26) Buda, F.; de Groot, H. J. M.; Bifone, A. *Phys. Rev. Lett*. **1996**, *77*, 4474−4477.
(27) Bifone, A.; de Groot, H. J. M.; Buda, F. *J. Phys. Chem. B* **1997**, *101*, 2954−2958.
(28) Bifone, A.; de Groot, H. J. M.; Buda, F. *Pure Appl. Chem*. **1997**, *69*, 2105−2110.
(29) La Penna, G.; Buda, F.; Bifone, A.; de Groot, H. J. M. *Chem. Phys. Lett.* **1998**, *294*, 447−453.
(30) Molteni, C.; Frank, I.; Parrinello, M. *J. Am. Chem. Soc*. **1999**, *121*, 12177−12183.
(31) Creemers, A. F. L.; Kiihne, S.; Bovee-Geurts, P. H. M.; de Grip, W. J.; Lugtenburg, J.; de Groot, H. J. M. *Proc. Natl. Acad. Sci. U.S.A.* **2002**, *99*, 9101−9106.
(32) Elia, G. R.; Childs, R. F.; Britten, J. F.; Yang, D. S. C.; Santarsiero, B. D. *Can. J. Chem*. **1996**, *74*, 591−601.
(33) Carravetta, M.; Zhao, X.; Johannessen, O. G.; Lai, C. W.; Verhoeven, M.; Bovee-Geurts, P. H. M.; Verdegem, P. J. E.; Kiihne, S.; Luthman, H.; de Groot, H. J. M.; de Grip, W. J.; Lugtenburg, J.; Levitt, M. H. *J. Am. Chem. Soc.* **2004**, *126*, 3948−3953.
(34) Parr, R. G.; Yang, W. *Density-Functional Theory of Atoms and Molecules*; Oxford University Press: New York, 1989.
(35) Perdew, J. P.; Zunger, A. *Phys. Rev. B* **1981**, *23*, 5048−5079.
(36) Becke, A. D. *Phys. Rev. A* **1988**, *38*, 3098−3100.
(37) Perdew, J. P. *Phys. Rev. B* **1986**, *33*, 8822−8824.
(38) Vanderbilt, D. *Phys. Rev. B* **1990**, *41*, 7892−7895.
(39) Jensen, F. *Introduction to Computational Chemistry*; John Wiley & Sons: Chichester, U.K., 1999.
(40) Wilson, E. B.; Decius, J. C.; Cross, P. C. *Molecular Vibrations*; Dover Publications Inc.: New York, 1980.
(41) Pulay, P. *J. Comput. Chem*. **1982**, *3*, 556−560.
(42) Becke, A. D. *J. Chem. Phys*. **1993**, *98*, 5648−5652.
(43) Lee, C.; Yang, W.; Parr, R. G. *Phys. Rev. B* **1988**, *37*, 785−789.
(44) Ditchfield, R. *Mol. Phys*. **1974**, *27*, 789−807.
(45) Hehre, W. J.; Ditchfield, R.; Pople, J. A. *J. Chem. Phys.* **1972**, *56*, 2257−2261.
(46) Touw, S. I. E.; Buda, F.; de Groot, H. J. M. To be published.
(47) Hutter, J.; Alavi, A.; Deutsch, T.; Bernasconi, M.; Goedecker, St.; Marx, D.; Tuckerman, M.; Parrinello, M. *CPMD*; MPI für Festkörperforschung and IBM Zürich Research Laboratory: Zürich, 1995−1999.
(48) Frisch, M. J.; Trucks, G. W.; Schlegel, H. B.; Scuseria, G. E.; Robb, M. A.; Cheeseman, J. R.; Zakrzewski, V. G.; Montgomery, J. A., Jr.; Stratmann, R. E.; Burant, J. C.; Dapprich, S.; Millam, J. M.; Daniels, A. D.; Kudin, K. N.; Strain, M. C.; Farkas, O.; Tomasi, J.; Barone, V.; Cossi, M.; Cammi, R.; Mennucci, B.; Pomelli, C.; Adamo, C.; Clifford, S.; Ochterski, J.; Petersson, G. A.; Ayala, P. Y.; Cui, Q.; Morokuma, K.; Malick, D. K.; Rabuck, A. D.; Raghavachari, K.; Foresman, J. B.; Cioslowski, J.; Ortiz, J. V.; Stefanov, B. B.; Liu, G.; Liashenko, A.; Piskorz, P.; Komaromi, I.; Gomperts, R.; Martin, R. L.; Fox, D. J.; Keith, T.; Al-Laham, M. A.; Peng, C. Y.; Nanayakkara, A.; Gonzalez, C.; Challacombe, M.; Gill, P. M. W.; Johnson, B. G.; Chen, W.; Wong, M. W.; Andres, J. L.; Head-Gordon, M.; Replogle, E. S.; Pople, J. A. *Gaussian 98*, revision A.5; Gaussian, Inc.: Pittsburgh, PA, 1998.
(49) Sugihara, M.; Buss, V.; Entel, P.; Elstner, M.; Frauenheim, T. *Biochemistry* **2002**, *41*, 15259−15266.
(50) Han, M.; DeDecker, S.; Smith, S. O. *Biophys. J*. **1993**, *65*, 899−906.
(51) Buss, V.; Sugihara, M.; Entel, P.; Hafner, J. *Angew. Chem., Int. Ed*. **2003**, *42*, 3245−3247.
(52) Röhrig, U. F.; Guidoni, L.; Rothlisberger, U. *Biochemistry* **2002**, *41*, 10799−10809.
(53) Nakanishi, K.; Crouch, R. *Isr. J. Chem*. **1995**, *35*, 253−272.
(54) Buss, V.; Kolster, K.; Terstegen, F.; Vahrenhorts, R. *Angew. Chem., Int. Ed*. **1998**, *37*, 1893−1895.
(55) Aton, B.; Doukas, A. G.; Callender, R. H.; Becher, B.; Ebrey, T. G. *Biochemistry* **1977**, *16*, 2995−2998.
(56) Mintmire, J. W.; White, C. T. *Phys. Rev. B* **1987**, *35*, 4180−4183.
(57) Vogel, P.; Campbell, D. K. *Phys. Rev. Lett*. **1989**, *62*, 2012−2015.
(58) Askenazi, J.; Picket, W. E.; Krakauer, H.; Wang, C. S.; Klein, B. M.; Chubb, S. R. *Phys. Rev. Lett.* **1989**, *62*, 2016−2019.
(59) van Gisbergen, S. J. A.; Schipper, P. R. T.; Gritsenko, O. V.; Baerends, E. J.; Snijders, J. G.; Champagne, B.; Kirtmab, B. *Phys. Rev. Lett*. **1999**, *83*, 694−697.
(60) Buda, F.; Giannozzi, P.; Mauri, F. *J. Phys. Chem. B* **2000**, *104*, 9048−9053.
(61) Buda, F.; Touw, S. I. E.; de Groot, H. J. M. In *Perspectives on Solid-State NMR in Biology*; Kiihne, S., de Groot, H. J. M., Eds.; Kluwer: Dordrecht, The Netherlands, 2001; pp 111−122.
(62) Nakayama, T. A.; Khorana, H. G. *J. Biol. Chem*. **1991**, *266*, 4269−4275.
(63) Terakita, A.; Yamashita, T.; Schichida, Y. *Proc. Natl. Acad. Sci. U.S.A.* **2000**, *97*, 14263−14267.
(64) Shriver, J. W.; Mateescu, G. D.; Abrahamson, E. W. *Biochemistry* **1979**, *18*, 4785−4792.
(65) de Groot, H. J. M. *Curr. Opin. Struct. Biol*. **2000**, *10*, 593−600.
(66) Boudreaux, D. S.; Chance, R. R.; Brédas, J. L.; Silbey, R. *Phys. Rev. B* **1983**, *28*, 258−267.
(67) Champagne, B.; Perpète, E. A.; van Gisbergen, S. J. A.; Baerends, E. J.; Snijders, J. G.; Soubra-Ghaoui, C.; Robins, K. A.; Kirtman, B. *J. Chem. Phys*. **1998**, *109*, 10489−10498.
(68) Kakitani, H.; Kakitani, T.; Rodman, H.; Honig, B. *J. Phys. Chem*. **1983**, *87*, 3620−3628.
(69) Curry, B.; Palings, I.; Broek, A. D.; Pardoen, J. A.; Lugtenburg, J.; Mathies, R. A. *Adv. Infrared Raman Spectrosc*. **1985**, *12*, 115−178.
(70) Warshel, A.; Karplus, M. J. *J. Am. Chem. Soc*. **1974**, *96*, 5677.
(71) Smith, S. O.; Myers, A. B.; Mathies, R. A.; Pardoen, J. A.; Winkel, C.; van den Berg, E. M. M.; Lugtenburg, J. *Biophys. J*. **1985**, *47*, 653−664.
(72) Smith, S. O.; Braiman, M. S.; Myers, A. B.; Pardoen, J. A.; Courtin, J. M. L.; Winkel, C.; Lugtenburg, J.; Mathies, R. A. *J. Am. Chem. Soc*. **1987**, *109*, 3108−3125.
(73) Lambert, J. B.; Shurvell, H. F.; Lightner, D. A.; Cooks, R. G. *Organic Structural Spectroscopy*; Prentice Hall: New York, 1998.